CHAPTER 5: METALLOINSERTION AT ABASIC SITES AND SINGLE BASE BULGES IN DNA[Φ]

5.1: INTRODUCTION

The maintenance of genomic integrity is critical to cellular health. However, a wide variety of agents, ranging from genotoxic chemicals to error-prone cellular polymerases, render DNA dangerously susceptible to damage and mutation.[1] The types of DNA defects are as varied as their causative agents, yet the most common forms are single base mismatches, abasic sites, single base bulges, and oxidized bases. Left unrepaired, all of these defects can lead to deleterious mutations, often in the form of single nucleotide polymorphisms.[2] To counter these threats, the cell has evolved complex DNA repair machineries, most notably the mismatch repair (MMR)[3−5] and base excision repair (BER)[6] pathways. Under normal conditions, the MMR (mismatches and single base bulges) and BER (abasic sites and oxidized bases) machineries will quickly and efficiently repair their target defects, thereby preventing any lasting damage to the cell or its genome. However, the suppression or disabling of these pathways is often met with dire consequences: mismatch repair deficiency, for example, has been implicated in 80% of hereditary non-polyposis colon cancers in addition to significant percentages of breast, ovarian, and skin cancers.[3, 7−10] It thus becomes clear that the synthesis and study of molecules able to specifically target these defects may aid in the development of new cancer diagnostics and therapeutics.

[Φ]Adapted from Zeglis, B. M.; Boland, J. A.; Barton, J. K. Targeting abasic sites and single base bulges in DNA with metalloinsertors. *J. Am. Chem. Soc.* **2008**, *130*, 7530−7531 and Zeglis, B. M.; Boland, J. A.; Barton, J. K. Recognition of abasic sites and single base bulges in DNA by a metalloinsertor. *Biochemistry* **2009**, *48*, 839−849.

As we have discussed in the preceding chapters, the design and application of metal complexes capable of specifically targeting one such defect, single base mismatches, have been focuses of our laboratory for over a decade.[11] These metal complexes, most notably $Rh(bpy)_2(chrysi)^{3+}$ (chrysi = chrysene-5,6-quinone diimine) and $Rh(bpy)_2(phzi)^{3+}$ (phzi = benzo[a]phenazine-5,6-quinone diimine) (**Figure 5.1**), bear sterically bulky ligands that are too wide to fit between matched base pairs and thus instead preferentially target thermodynamically destabilized mismatched sites.[12, 13] The compounds are highly specific ($\geq$ 1000-fold) for mispaired sites over matched base pairs and recognize over 80% of mismatches in all possible sequence contexts, with only thermodynamically stable, G-containing mismatches escaping binding altogether.[14−16] Furthermore, the complexes can, upon irradiation with ultraviolet light, promote direct cleavage of the DNA backbone at the binding site.

More recently, crystallography and NMR studies have revealed that these complexes do not bind their target sites via classical intercalation, in which the complex binds from the major groove and increases the base pair rise by stacking an aromatic ligand between intact base pairs. Rather, they employ a unique binding mode that we have termed metalloinsertion, in which the complex binds from the minor groove, ejecting the mismatched bases into the major groove and replacing them in the base stack with the sterically expansive aromatic ligand (**Figure 5.2**).[17, 18] These structural data make quite clear the origin of the correlation between recognition and thermodynamic destabilization: the less stable the mismatch, the easier the ejection of the mismatched bases.

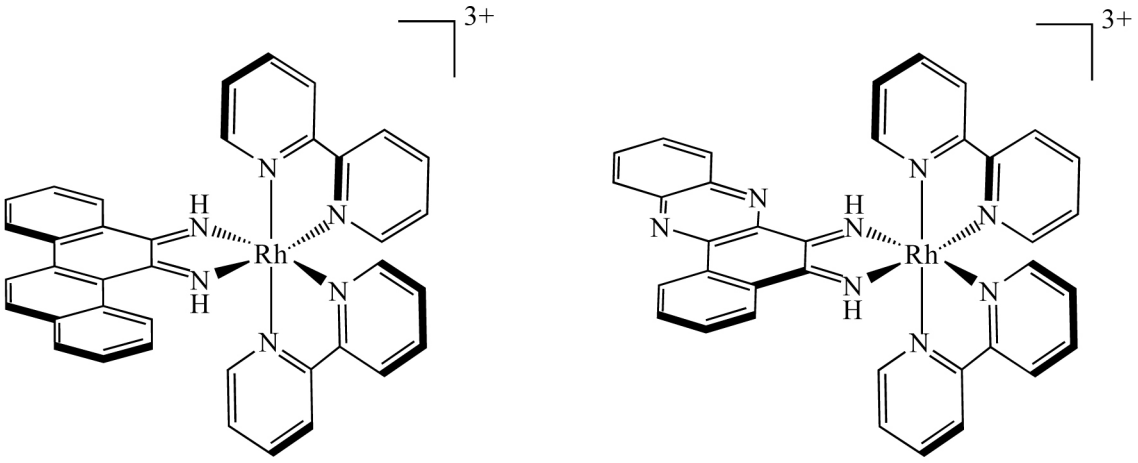

Δ-Rh(bpy)$_2$(chrysi)$^{3+}$ Δ-Rh(bpy)$_2$(phzi)$^{3+}$

Figure 5.1: Structures of two mismatch-specific metalloinsertors. The Δ-enantiomers of Rh(bpy)$_2$(chrysi)$^{3+}$ (left) and Rh(bpy)$_2$(phzi)$^{3+}$ (right) are shown; each complex bears two 2,2'-dipyridine ligands and a sterically expansive inserting ligand.

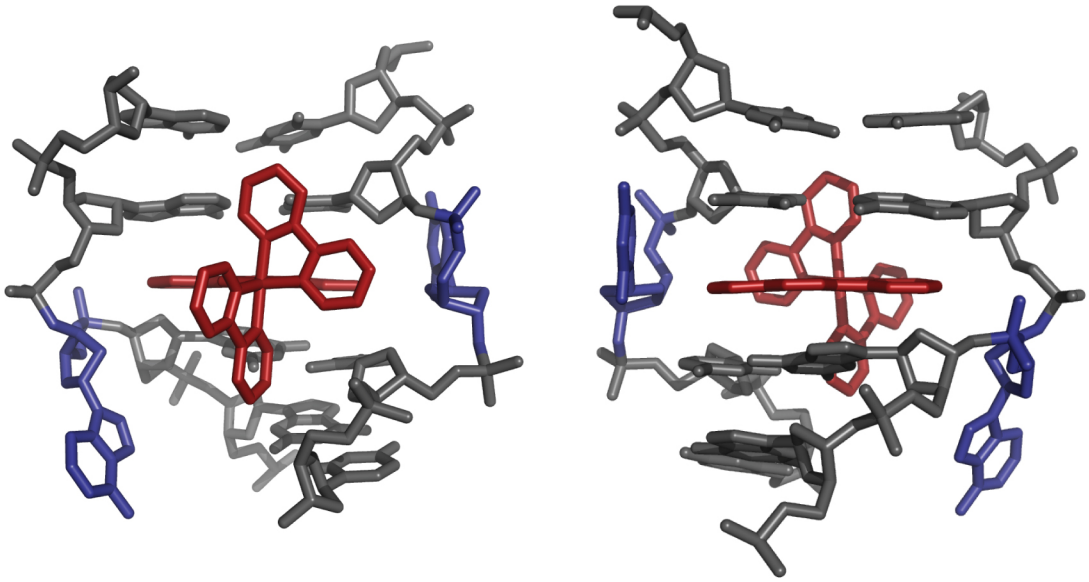

Figure 5.2: Crystal structure of metalloinsertion at a C•A mismatch.[18]
Metalloinsertion of $Rh(bpy)_2(chrysi)^{3+}$ at a C•A mispair as viewed from the minor (left) and major (right) sides of the duplex; the metal complex approaches the DNA from the minor groove, ejects the mispaired bases, and replaces them in the π-stack with the sterically expansive chrysi ligand.

Yet mismatches are not the only destabilizing DNA defect. Indeed, far from it. Consequently, the relationship between thermodynamic instability and metalloinsertor binding has led our laboratory to investigate the recognition of two different DNA defects: abasic sites and single base bulges.

Abasic sites arise from the cleavage of the glycosidic bond between the ribose and the nucleobase. This can occur spontaneously, as a result of exogenous agents, or as an intermediate in the BER pathway (**Figure 5.3**).[19, 20] Regardless of their source, abasic sites are among the most common DNA defects *in vivo*. Understandably, the exact numbers have proven difficult to predict and even harder to determine experimentally; however, data from *in vitro* studies have suggested that in human cells, as many as 10,000 abasic sites per cell cycle can be formed by spontaneous depurination *alone*.[21]

In the cell, abasic sites exist as a 40:60 mixture of α- and β-hemiacetal anomers in equilibrium with a minor ring-opened aldehylic form that represents less than 1% of total sites (**Figure 5.4a**).[22] Just as important to the structure of the defect site, however, is the unpaired base complementary to the abasic ribose. Numerous structural studies have shown that the conformation of this unpaired base can be extra- or intrahelical depending upon its identity and that of the surrounding bases (**Figure 5.5a**).[23−28] Unpaired purines are almost always intrahelical, whereas unpaired pyrimidines likely exist in equilibrium between extrahelical and intrahelical forms, with the extrahelical form favored when the base is flanked by other pyrimidines. Relative to intact duplex DNA, duplexes containing abasic sites are thermodynamically destabilized by 3−11 kcal/mol.[29, 30] Both the sequence context and the identity of the unpaired base play roles in the magnitude of the

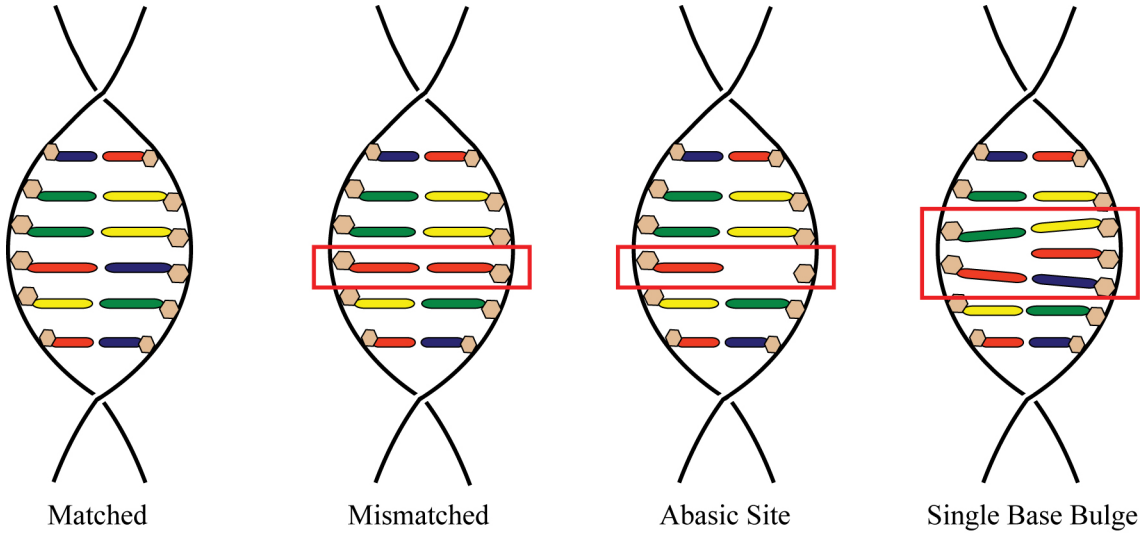

Figure 5.3: Schematic illustration of DNA defect sites. While both abasic sites and single base bulges are characterized by an unpaired base, the local environment of said base differs considerably in each case.

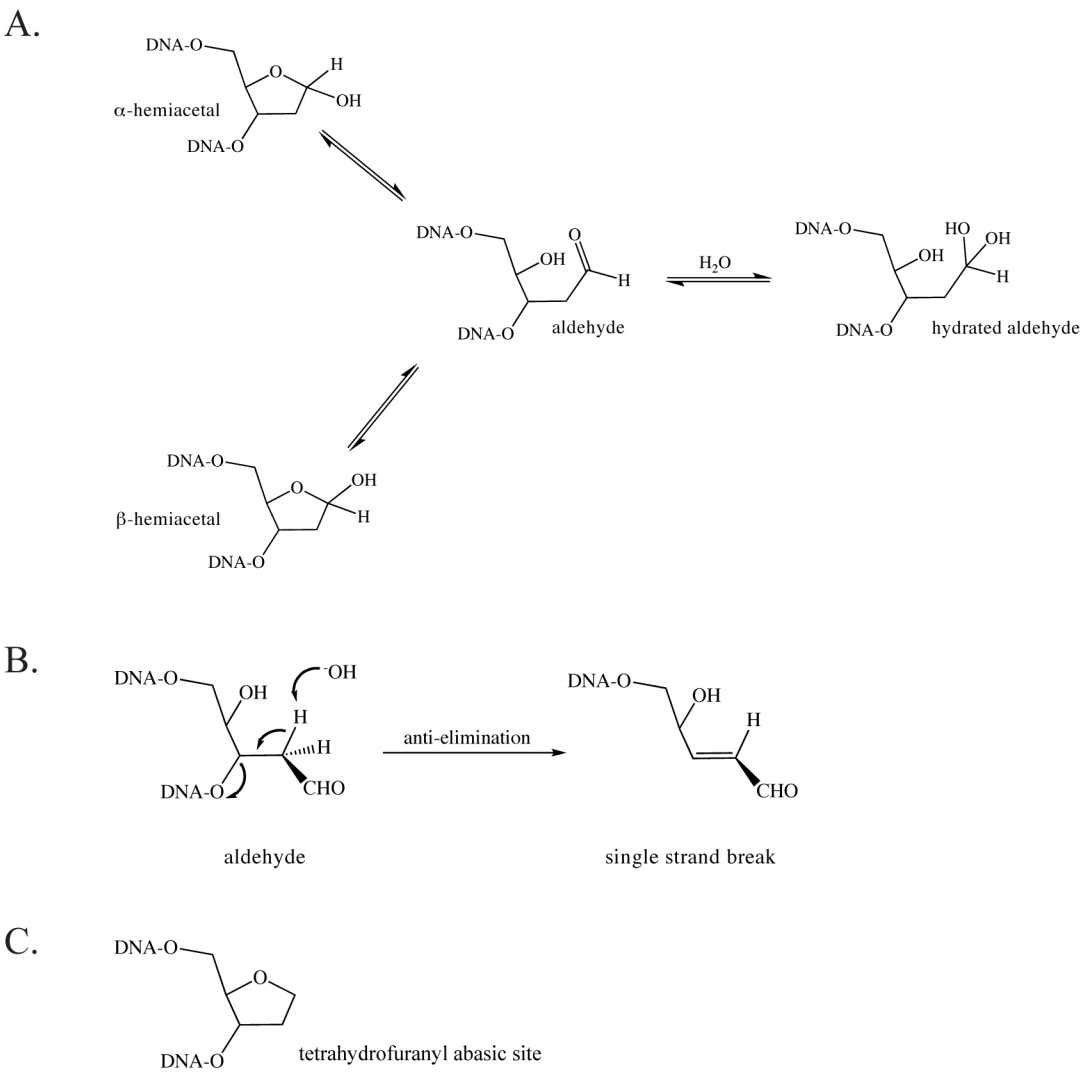

Figure 5.4: The structure and chemistry of abasic sites. (A) Illustration of the equilibrium of abasic sites between the two major hemiacetal anomers and the minor aldehylic and hydrated aldehylic forms. (B) The anti-elimination mechanism of single strand break formation at an aldehylic abasic site. (C) The synthetic tetrahydrofuranyl abasic site

destabilization. Sites in which the abasic ribose is flanked by purines are more stable than those flanked by pyrimidines, and, to a lesser degree, sites with unpaired purines are more stable than those with unpaired pyrimidines.

Single base bulges are defects in which a nucleotide is inserted in one strand of an otherwise well matched duplex (**Figure 5.3**). Caused by errors in recombination and replication, these sites are more thermodynamically stable than abasic sites, with destabilizations ranging from 0−3 kcal/mol.[31] Recent computational and spectroscopic studies have shown that while bulged base identity and sequence context certainly influence the destabilization of the site, reliable patterns such as those for abasic sites do not exist.[32, 33] Several structural studies have shown that the unpaired base may be intra- or extrahelical (**Figure 5.5b**).[34−41] Similar to the case for abasic sites, unpaired purines are almost always intrahelical, whereas an equilibrium between intra- and extrahelical conformations is likely for unpaired pyrimidines. Further, unpaired bases flanked by purines are more likely to remain intrahelical than those surrounded by pyrimidines. Regardless of unpaired base helicity, all duplexes with single base bulges are bent relative to well-matched DNA.

Under normal conditions, abasic sites and single base bulges are repaired through the BER and MMR pathways, respectively. However, if left unrepaired, both lesions represent significant threats to cell viability. Abasic sites can lead to single nucleotide polymorphisms, block transcription, inhibit DNA replication, and act as potent topoisomerase poisons.[19, 20, 42] Single base bulges, in contrast, are a very common source of frame-shift mutations.[43] Indeed, deficiency in the repair of both types of defects has been associated with several different cancers. MMR-deficiency (*vide supra*) has been

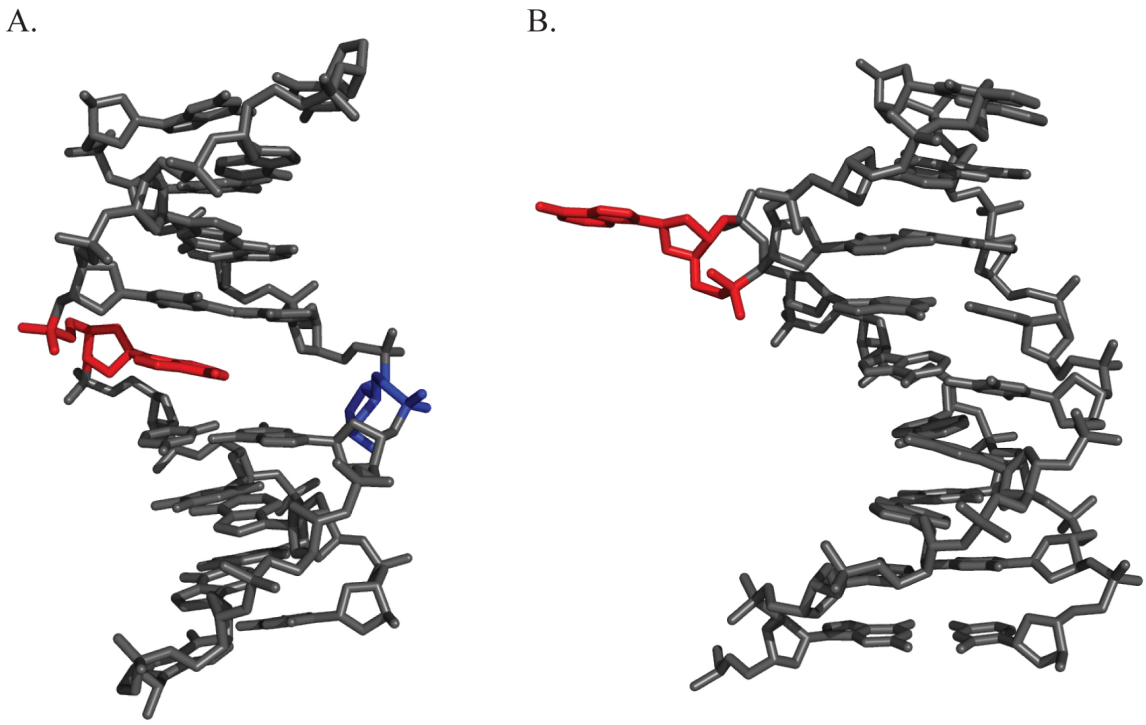

Figure 5.5: Structures of an abasic site and a single base bulge. (A) The NMR solution structure of an intrahelical adenosine opposite an abasic site.[27] (B) The X-ray crystal structure of an extrahelical adenosine single base bulge[36]; it is important to note that while this bulged adenosine adopts an extrahelical conformation, most solution evidence suggests that bulged purines adopt intrahelical conformations.

linked to hereditary non-polyposis colon, ovarian, breast, and skin cancers, while BER-deficiency has been implicated in types of colorectal and gastric cancers.[6, 44, 45]

Given these well-established links to cancer, it is not surprising that agents that recognize these lesions have already been designed and studied (**Figure 5.6**). Methodologies for the targeting of abasic sites include organic base substitute-intercalator conjugates[46] and nucleophilic amines that react with the minor aldehylic form of the natural abasic site.[47] Bulge recognition agents present a more diverse picture: naphthyridine derivatives[48–50], octahedral cobalt complexes[51], and dinuclear ruthenium compounds[52, 53] have all been shown to bind single or multiple base bulges along with DNA hairpins. Of particular interest here is the anti-tumor drug neocarzinostatin chromophore (NCS-Chrom, **Figure 5.6e)**, a member of the enediyne family of molecules.[54–57] NCS-Chrom binds single base bulges in duplex DNA via the minor groove with promising specificity and, upon activation with thiol, undergoes a transformation to a reactive biradical species that can cleave the DNA at the binding site. The success of NCS-Chrom not withstanding, almost all of these recognition agents exhibit affinities, specificities, or reactivities that are less than ideal for diagnostic or therapeutic applications.

Our investigation of metalloinsertors for abasic site and single base bulge recognition is thus motivated both by the desire to augment our understanding of the recognition of DNA lesions by metal complexes and by the opportunity to create useful diagnostic agents for the detection of these two deleterious defects.

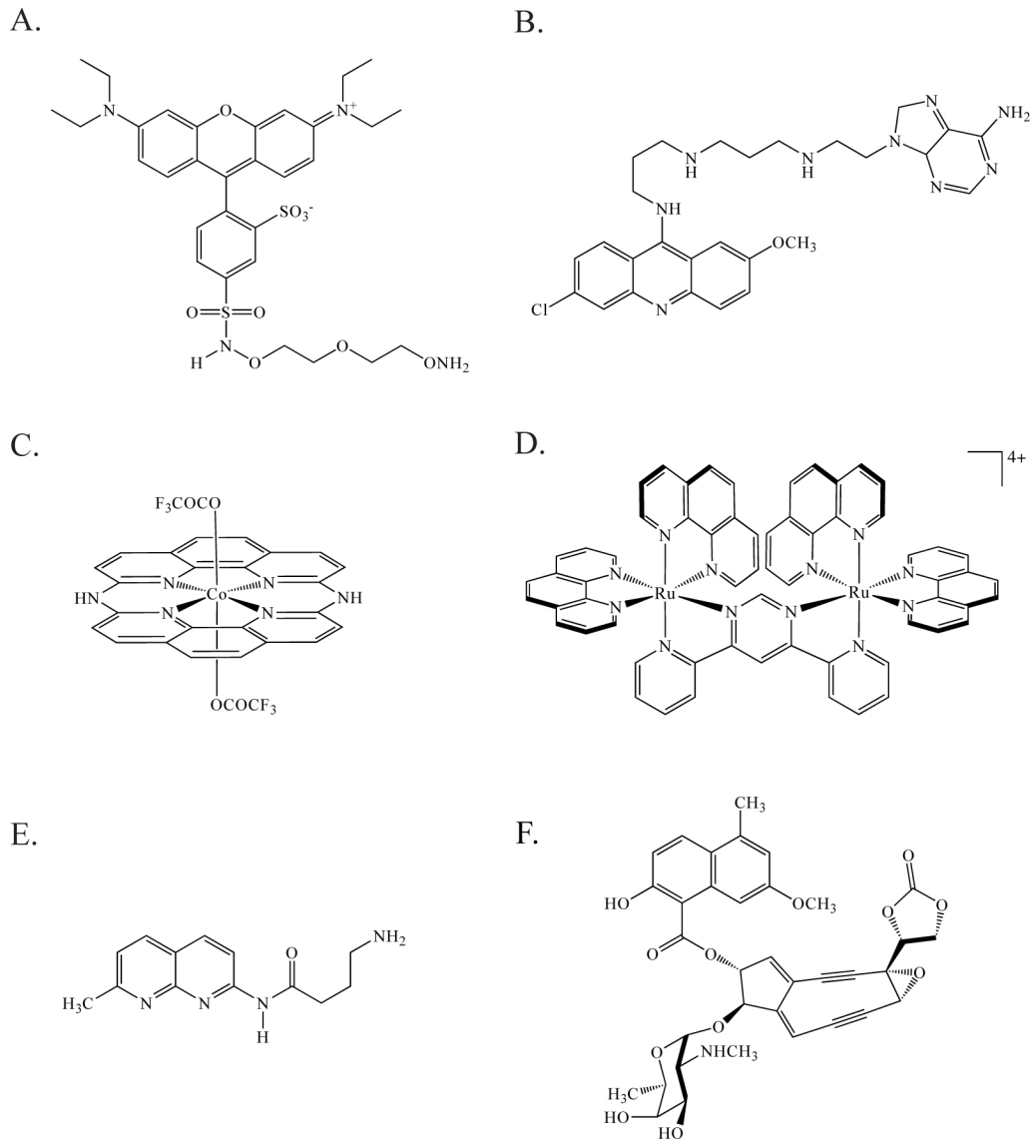

Figure 5.6: Abasic site and bulge recognition agents. For abasic sites: (A) fluorophore-conjugated nucleophilic amine[47]; (B) base analogue-intercalator conjugate[46]. For bulges: (C) octahedral cobalt complex[51]; (D) dinuclear ruthenium polypyridyl complex[52]; (E) naphthyridine derivative[49]; (F) neocarzinostatin chromophore[56]

5.2: RESULTS

5.2.1: SEQUENCE DESIGN AND MELTING TEMPERATURE ANALYSIS

A series of oligonucleotides was synthesized and purified to allow for the interrogation of abasic sites and single base bulges in variable sequence contexts and with all possible unpaired bases. The 27-mer single strands are identical except for a central six base region in which the sequence variation occurs. Four different oligonucleotides containing synthetic abasic sites were designed, each placing the abasic site in a different sequence context: 5'-GΦT-3' (AB1), 5'-GΦA-3' (AB2), 5'-AΦG-3' (AB3), and 5'-TΦC-3' (AB4) (**Table 5.1**). For each abasic strand, four complements were prepared. Each positions a different base complementary to the abasic site: for example, 3'-C*A*A-5' (AB1-A), 3'-C*C*T-5' (AB2-C), 3'-T*G*C-5' (AB3-G), and 3'-A*T*G-5' (AB4-T). These oligonucleotides, taken together, allow us to examine the recognition of abasic sites in the three major sequence context types (5'-PurΦPur-3', 5'-PyrΦPur-3', 5'-PyrΦPyr-3') with all possible opposing unpaired bases. For purposes of comparison, matched and mismatched strands were also created for each sequence context; complementary in each case to the AB#-C strand, these oligonucleotides create either a fully matched duplex or one containing a central C•C mismatch.

Four additional oligonucleotides were synthesized to facilitate the study of single base bulges (**Table 5.2**). These, termed B1−B4, are identical to the AB# strands in all respects except that they lack the tetrahydrofuranyl abasic site. Thus, when these 26-mers are annealed to the 27-mer complements of the abasic oligonucleotides, duplexes with single base bulges are formed. In each case, the nucleotide formerly complementary to the abasic site is now the bulged base: for example, 3'-C*T*A-5' (B1-T), 3'-C*A*T-5' (B2-

A), 3’-T*C*C-5’ (B3-C), and 3’-A*G*G-5’ (B4-G). The same sets of matched and mismatched duplexes were employed as controls. In all, 32 oligonucleotides forming 28 unique duplexes were created.

Melting temperature analysis of the DNA allows us to determine the relative thermodynamic destabilization to the duplex created by each lesion. All four matched duplexes have melting temperatures around 64 °C. Relative to these, the mismatched duplexes are destabilized by 7−8 °C. Duplexes containing single base bulges are similarly destabilized, if not slightly more stable, with melting temperatures 6−8 °C lower than that of the corresponding matched duplex. In contrast, duplexes containing abasic sites are even less stable than their mismatched counterparts, with melting temperatures reduced by 8−11 °C. Taken together, these ΔT_m values are in agreement with the published literature It is somewhat surprising, however, that within the family of abasic duplexes, we do not see significant variation in ΔT_m based upon sequence context or unpaired base identity. This result is more likely a product of instrument sensitivity than an indicator of the absence of such influences on site stability. Nonetheless, these measurements plainly illustrate the relative stabilities of the sites at hand: abasic site < mismatched base pair < single base bulge << matched base pair.

Sequence	Seq. Variation[a]	Context	Recognition[b]	K_B(10^6 M^{-1})[c]	T_m(°C)[d]
AB1-M	GGGTGA CCCACT	–	–	–	64.5
AB1-MM	GGCTGA CCCACT	5′-PurCPyr-3′ 3′-PyrCPur-5′	Yes	2.2(2)	57.0
AB1-X	GGΦTGA[e] CCXACT[f]	5′-PurΦPyr-3′ 3′-PyrXPur-5′	X = A: Yes, C: Yes, G: Yes, T: Yes	A: 1.3(1) C: 2.3(5) G: 1.4(2) T: 3.9(6)	A: 56.0 C: 56.0 G: 57.0 T: 55.5
AB2-M	GGATGA CCTACG	–	–	–	64.0
AB2-MM	GCATGA CCTACT	5′-PurCPur-3′ 3′-PyrCPyr-5′	Yes	1.7(2)	56.5
AB2-X	GΦATGA CXTACT	5′-PurΦPur-3′ 3′-PyrXPyr-5′	X = A: Yes, C: Yes, G: Yes, T: Yes	A: 2.1(1) C: 2.6(5) G: 1.4(5) T: 3.5(3)	A: 54.0 C: 53.5 G: 55.0 T: 54.5
AB3-M	GGAGGA CCTCCT	–	–	–	64.0
AB3-MM	GGACGA CCTCCT	5′-PurCPur-3′ 3′-PyrCPyr-5′	No	–	56.0
AB3-X	GGAΦGA CCTXCT	5′-PurΦPur-3′ 3′-PyrXPyr-5′	X = A: No, C: No, G: No, T: No	–	A: 55.5 C: 55.0 G: 56.0 T: 56.0
AB4-M	TGCTGA ACGACT	–	–	–	64.0
AB4-MM	TCCTGA ACGACT	5′-PyrCPyr-3′ 3′-PurCPur-5′	Yes	2.5(3)	56.0
AB4-X	TΦCTGA AXGACT	5′-PyrΦPyr-3′ 3′-PurXPur-5′	X = A: Yes, C: Yes, G: Yes, T: Yes	A: 1.2(3) C: 2.9(4) G: 1.7(1) T: 3.1(5)	A: 54.5 C: 53.5 G: 54.5 T: 53.0

a. Sequence within variable region of 5′-GAC TTA TCT AG*N NNN NN*T AAG CTG GTC-3′ (top) and complement (bottom).
b. Determined by photocleavage assay employing 1 μM $Rh(bpy)_2(chrysi)^{3+}$ and 1μM duplex DNA in buffer (50 mM NaCl, 10 mM NaPi, pH 7.1).
c. Measured via binding titration experiment using 1 μM duplex DNA and variable concentrations (0-20 μM) of $Rh(bpy)_2(chrysi)^{3+}$ in buffer.
d. Determined with UV-Visible spectrophotometry employing 1 μM duplex DNA in buffer. Accurate within 1 °C.
e. Φ denotes tetrahydrofuranyl abasic site.
f. X denotes base complementary to abasic site.

Table 5.1: Sequence and recognition information for abasic assemblies

Sequence[a]	Seq. Variation[b]	Context	Recognition[c]	T_m (°C)[d]
B1-X	GG TGA CC X ACT[e]	5′-Pur Pyr-3′ 3′-Pyr X Pur-5′	X = A: No C: Yes G: Yes T: Yes	A: 58.0 C: 59.0 G: 59.0 T: 59.0
B2-X	G ATGA C X TACT	5′-Pur Pur-3′ 3′-Pyr X Pyr-5′	X = A: Yes C: Yes G: Yes T: Yes	A: 56.0 C: 57.0 G: 57.5 T: 57.5
B3-X	GGA GA CCT X CT	5′-Pur Pur-3′ 3′-Pyr X Pyr-5′	X = A: No C: No G: No T: No	A: 55.5 C: 55.0 G: 56.0 T: 56.0
B4-X	T CTGA A X GACT	5′-Pyr Pyr-3′ 3′-Pur X Pur-5′	X = A: No C: No G: No T: No	A: 57.0 C: 56.4 G: 57.0 T: 57.0

a. Data for the corresponding matched and mismatched strands (e.g. AB1-M and AB1-MM for B1-X) can be found in Table 1.
b. Sequence within variable region of 5′-GAC TTA TCT AG*N NNN NN*T AAG CTG GTC-3′ (top) and complement (bottom). The complement contains the bulged base.
c. Determined by photocleavage assay employing 5 μM $Rh(bpy)_2(chrysi)^{3+}$ and 1μM duplex DNA in buffer (50 mM NaCl, 10 mM NaPi, pH 7.1).
d. Determined with UV-Visible spectrophotometry employing 1 μM duplex DNA in buffer. Accurate within 1 °C.
e. X denotes the bulged base.

Table 5.2: Sequence and recognition information for single base bulge assemblies

5.2.2: Recognition of abasic sites by $Rh(bpy)_2(chrysi)^{3+}$

Polyacrylamide gel electrophoresis experiments clearly indicate that $Rh(bpy)_2(chrysi)^{3+}$ specifically recognizes and photocleaves abasic sites in DNA (**Figure 5.7**). Indeed, the metalloinsertor binds and promotes strand scission at lesion sites in all sequence context types (5'-PurΦPur-3', 5'-PurΦPyr-3', and 5'-PyrΦPyr-3') and with all possible unpaired bases. No photocleavage is observed in the absence of metalloinsertor or with well-matched DNA. In total, twelve of the sixteen abasic sites are bound and cleaved. Specifically, the abasic sites in duplexes AB1, AB2, and AB4 are recognized and cleaved regardless of unpaired base identity; surprisingly, however, no photocleavage is observed for the AB3 duplexes. This pattern corresponds precisely to that observed for the strands bearing a central C•C mismatch: AB1-MM, AB2-MM and AB4-MM are all bound and cleaved, while AB3-MM escapes binding and scission. That the AB3 duplexes are not bound and cleaved is certainly not a consequence of the sequence context type; the AB2 duplexes, like the AB3 assembles, place the abasic site in a 5'-PurΦPur-3' sequence context and are, in fact, cleaved quite readily. The answer likely lies in the sensitivity of metalloinsertors to specific sequence contexts. Similar effects of sequence context have been seen previously for the family of complexes with mismatched duplexes.[11] Indeed, experiments employing higher rhodium concentrations and longer irradiation times suggest that $Rh(bpy)_2(chrysi)^{3+}$ does bind and cleave the abasic sites in the AB3 duplexes, just not nearly as strongly or efficiently as those in the other sequence contexts.

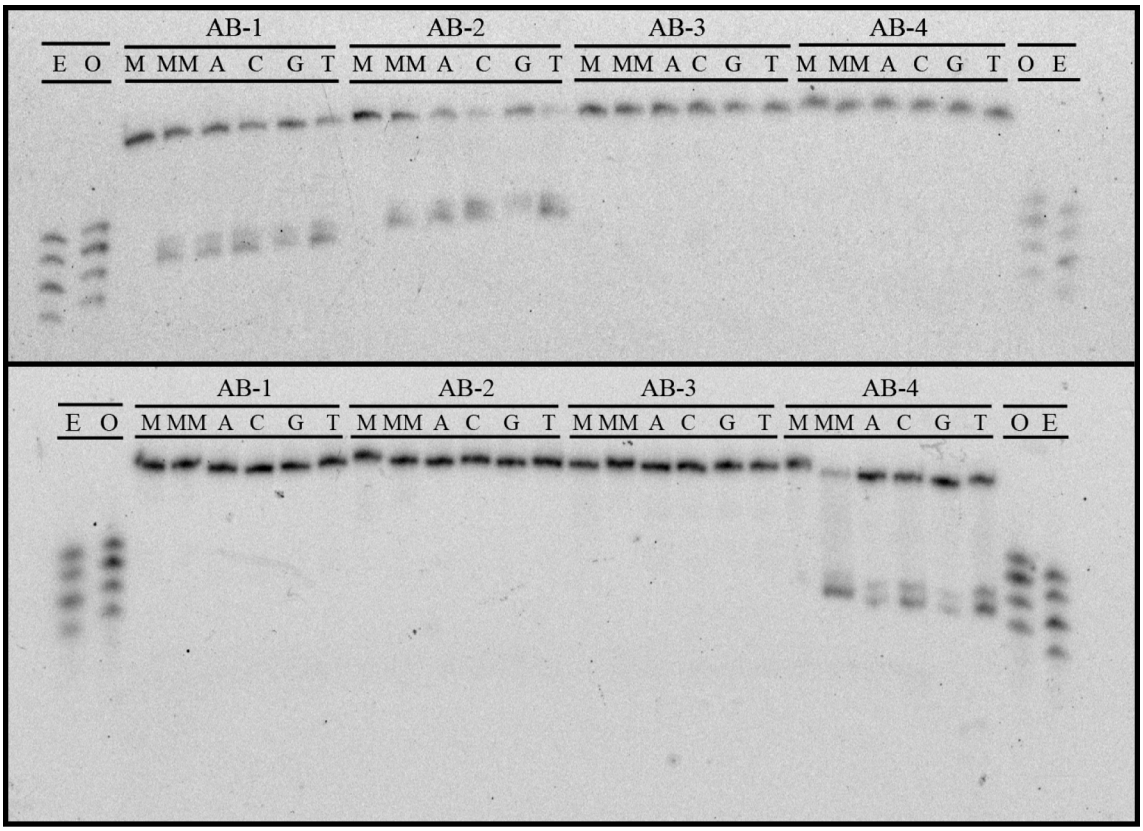

Figure 5.7: Abasic site recognition and photocleavage gel. PAGE assay illustrating the recognition and photocleavage of mismatch and abasic site recognition. Sequence contexts are listed along top line of each gel, and individual duplexes are indicated in the second line (M = matched, MM = mismatched, A = unpaired adenine, C = cytosine, G = guanine, and T = thymine). In the top gel, the single strand beginning 5'-GAC CAG … (that containing the unpaired base in the abasic assemblies) is 5'-^{32}P-labeled. In the bottom gel, the single strand beginning 5'-GAC TTA … (that containing the abasic site) is 5'-^{32}P-labeled. In both experiments, 1 μM duplex was incubated with $Rh(bpy)_2(chrysi)^{3+}$ in 50 mM NaCl, 10 mM NaPi, pH 7.1. Samples were irradiated for 10 min on an Oriel Instruments solar simulator (320−440 nm emission) and incubated for 30 min at 60 °C prior to electrophoresis. "E" and "O" denote lanes containing even (10, 12, 14, 16) and odd (11, 13, 15, 17) standardization fragments.

Photocleavage experiments also reveal interesting patterns in the strand asymmetry of scission. Regardless of the identity of the unpaired base, duplexes AB1 and AB2 are cleaved on the strand containing the unpaired nucleotide. Interestingly, however, duplex AB4 is cleaved instead on the strand containing the tetrahydrofuranyl abasic site, again irrespective of the unpaired base. This behavior exactly mirrors the photocleavage observed in the analogous mismatched duplexes. While, of course, the mismatched duplexes contain no unpaired bases or abasic sites, the AB1-MM and AB2-MM assemblies are cleaved on the strand corresponding to that containing an unpaired base in the abasic duplexes, and the AB4-MM assembly is cleaved on the strand corresponding to that containing the abasic site in the abasic duplex. This observation must reflect the binding architecture of the complex in the abasic site (see Discussion).

Another important similarity between photocleavage at mismatch and abasic sites is the length of the scission products. Regardless of unpaired base identity, AB1 cleavage fragments are 14 base pairs long, AB2 fragments 15 base pairs long, and AB4 fragments 13 base pairs long. These fragments correspond to cleavage at the ribose 3' to the unpaired base in duplexes AB1 and AB2 and at the ribose 3' to the abasic site in the AB4 duplexes. Importantly, photocleavage at the C•C mismatch in each duplex produces fragments of analogous lengths.

5.2.3: Recognition of abasic sites by $Rh(bpy)_2(phzi)^{3+}$

In order to probe the generality of metalloinsertor recognition of abasic sites, photocleavage experiments were also performed using $Rh(bpy)_2(phzi)^{3+}$, a second generation complex with a heterocyclic bulky ligand (**Figure 5.1**). $Rh(bpy)_2(phzi)^{3+}$ is

clearly able to both recognize and, upon irradiation, cleave the representative abasic sites (**Figure 5.8**). Again, no recognition or photocleavage is observed in the absence of metalloinsertor or DNA defect. Significantly, photocleavage with $Rh(bpy)_2(phzi)^{3+}$ is observed at much lower concentrations (100 nM) than with $Rh(bpy)_2(chrysi)^{3+}$, a characteristic also observed for mismatch photocleavage and attributed to the added π-stacking capabilities of the heterocyclic inserting ligand.

5.2.4: BINDING AFFINITIES OF $RH(BPY)_2(CHRYSI)^{3+}$ FOR ABASIC SITES

Photocleavage titration experiments were employed to determine site-specific binding constants for the twelve abasic sites and three mismatches for which photocleavage was observed (**Figure 5.9** shows a representative titration, see also **Table 5.1**). The binding constants for the mismatched sites, 2.2(2) x 10^6 M^{-1} (AB1-MM), 1.7(2) x 10^6 M^{-1} (AB2-MM), 2.5(3) x 10^6 M^{-1} (AB4-MM), are comparable to those previously reported for C•C mismatches.[11] Since metalloinsertor binding affinity correlates directly to site destabilization, it is not surprising that the binding constants of $Rh(bpy)_2(chrysi)^{3+}$ for abasic sites are similar to if not somewhat greater than those for the most destabilizing (e.g., C•C) mismatches.

Despite probable differences in site destabilization between the three different sequence contexts, little variation is observed in the affinity values, a result that suggests a threshold behavior in the relationship between destabilization and binding affinity. Such behavior has previously been suggested for mismatch binding.[11] Small differences, however, do appear based on the identity of the unpaired base within a single sequence

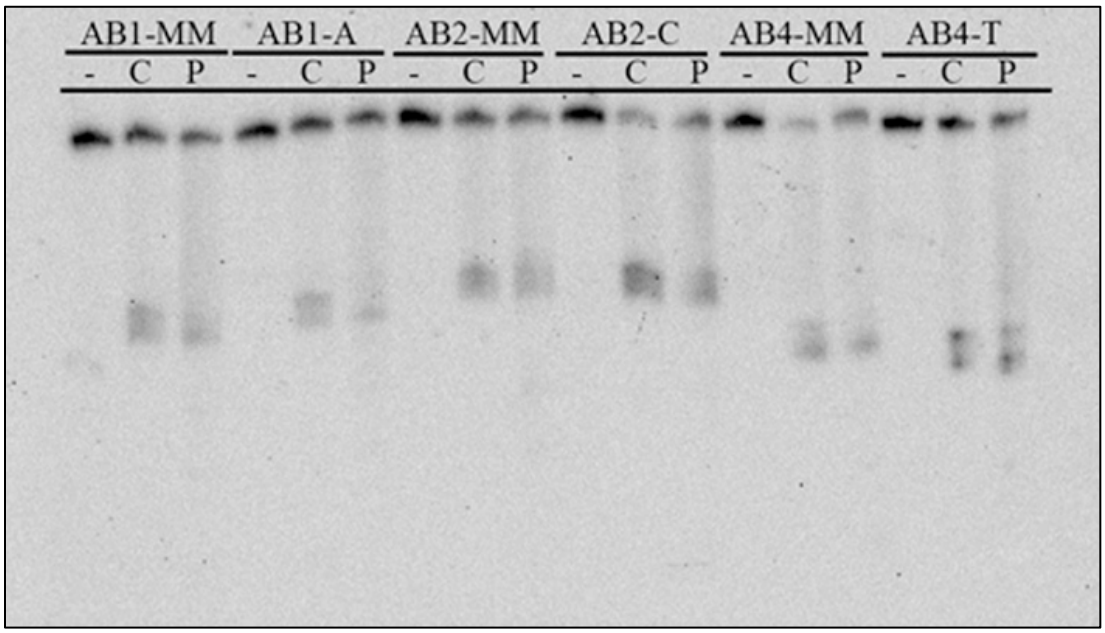

Figure 5.8: Recognition of abasic sites with $Rh(bpy)_2(phzi)^{3+}$. PAGE assay illustrating the recognition and photocleavage of mismatches and abasic sites by $Rh(bpy)_2(chrysi)^{3+}$ and $Rh(bpy)_2(phzi)^{3+}$. 1 μM duplex was incubated without metal complex (lanes marked "–") , with 1 μM $Rh(bpy)_2(chrysi)^{3+}$ (lanes marked "C"), or with 100 nM $Rh(bpy)_2(phzi)^{3+}$ (lanes marked "P") in 50 mM NaCl, 10 mM NaPi, pH 7.1. Duplex identity is indicated at the top of the gel. Samples were irradiated for 10 min on an Oriel Instruments solar simulator (320−440 nm emission) and incubated for 30 min at 60 °C prior to electrophoresis.

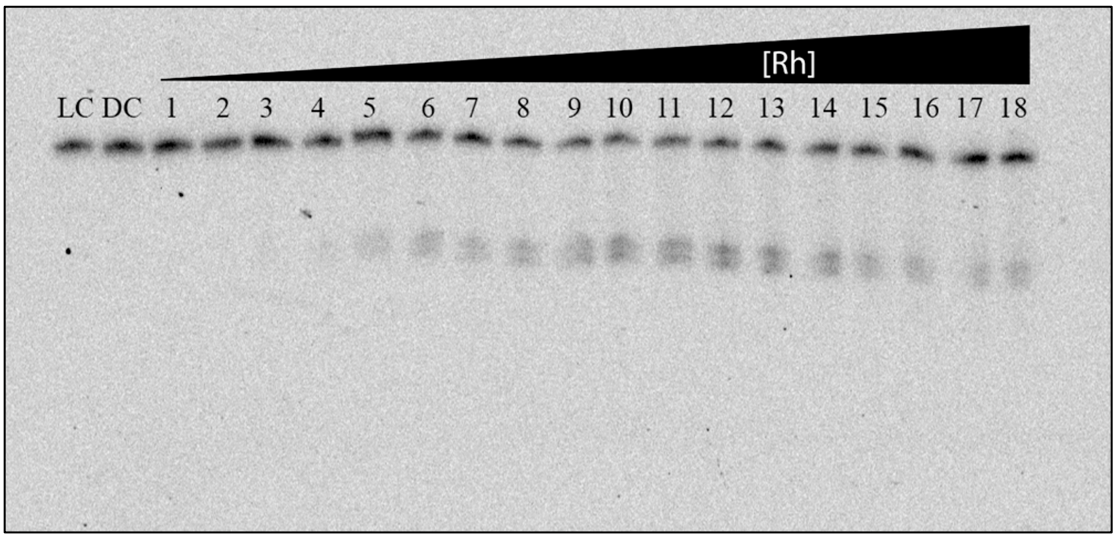

Figure 5.9: Determining the binding constant of $Rh(bpy)_2(chrysi)^{3+}$ for an abasic site. PAGE assay illustrating a typical photocleavage assay for binding constant determination. 1 μM duplex was incubated with increasing concentrations of $Rh(bpy)_2(chrysi)^{3+}$ in 50 mM NaCl, 10 mM NaPi, pH 7.1. The AB1-C duplex was employed for this particular titration. Samples were irradiated for 10 min on an Oriel Instruments solar simulator (320−440 nm emission) and incubated for 30 min at 60 °C prior to gel electrophoresis. LC and DC represent light (no rhodium, 10 min irradiation) and dark (1 μM Rh, no irradiation) controls. Lanes 1−18 contain 50 nM, 100 nM, 200 nM, 300 nM, 400 nM, 500 nM, 600 nM, 700 nM, 800 nM, 1 μM, 2 μM, 3 μM, 4 μM, 5 μM, 7 μM, 9 μM, 13 μM, 15μM, 17.5 μM, 20 μM $Rh(bpy)_2(chrysi)^{3+}$.

context. For example, the values for the AB2 assemblies are 1.4(5) x 10^6 M^{-1} (G), 2.1(1) x 10^6 M^{-1} (A), 2.6(5) x 10^6 M^{-1} (C), and 3.5(3) x 10^6 M^{-1} (T). The metalloinsertor seems to bind abasic sites with unpaired pyrimidines slightly tighter than sites with unpaired purines. These differences are admittedly minor; however, the trend is consistent among the three sequence contexts. An explanation based on the dynamic motions and helicity of the unpaired base in each case is perhaps most likely.

5.2.5: ENANTIOSPECIFICITY OF $Rh(bpy)_2(chrysi)^{3+}$ FOR ABASIC SITES

Photocleavage assays employing Δ-$Rh(bpy)_2(chrysi)^{3+}$ and Λ-$Rh(bpy)_2(chrysi)^{3+}$ clearly indicate that abasic recognition is enantiospecific for the right-handed isomer of the metalloinsertor (**Figure 5.10**). PAGE experiments reveal that concentrations of 1 μM Δ-$Rh(bpy)_2(chrysi)^{3+}$ bind and cleave all abasic sites interrogated, while incubation and irradiation with 1 μM Λ-$Rh(bpy)_2(chrysi)^{3+}$ produces no photocleavage bands. This chiral specificity has been well-documented for the recognition of mismatched sites by metalloinsertors.[62] Recent structural studies of $Rh(bpy)_2(chrysi)^{3+}$ bound to a C•A mismatch have shed light on the question; because the metalloinsertor binds the mismatch site from the narrow, sterically constrictive minor groove, the chirality of complex must match that of the helix to prevent steric clash between the ancillary ligands and the DNA backbone. In short, the right-handed helix can only accommodate the right-handed enantiomer. The observation that the recognition of abasic sites by metalloinsertors is also enantiospecific argues strongly for site binding via the minor groove.

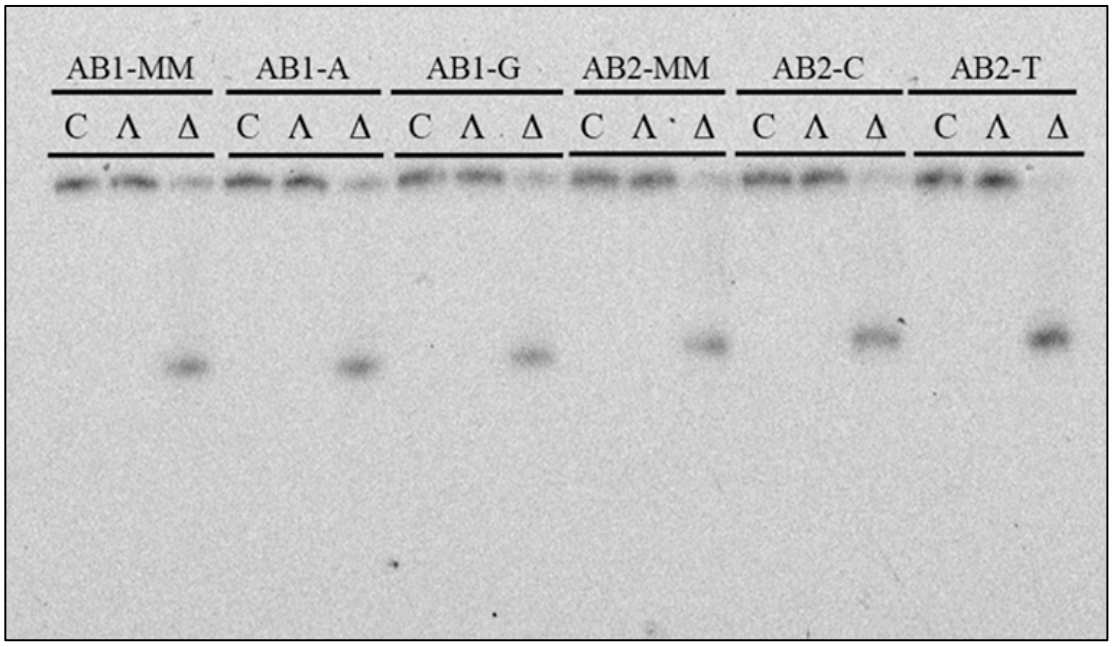

Figure 5.10: The enantiospecificity of abasic site recognition. PAGE assay illustrating the enantioselectivity of mismatch and abasic site recognition. 1 μM duplex was incubated with either Δ-$Rh(bpy)_2(chrysi)^{3+}$, Λ-$Rh(bpy)_2(chrysi)^{3+}$, or no Rh complex at all in 50 mM NaCl, 10 mM NaPi, pH 7.1. Samples were irradiated for 10 min on an Oriel Instruments solar simulator (320−440 nm emission) and incubated for 30 min at 60 °C prior to electrophoresis.

5.2.6: MALDI-TOF analysis of abasic site photocleavage products

While we have predominantly employed gel electrophoresis in our study of the recognition of abasic sites, MALDI-TOF mass spectrometry affords a unique opportunity to investigate not only the site specificity of recognition but also the identity of the individual photocleavage products.[63] A similar investigation has been previously reported for the recognition of mismatched sites. Here, the photocleavage of all 12 cleaved abasic duplexes and their mismatched analogues was investigated. The MALDI-TOF analysis of AB1-C photocleavage provides a suitable example (**Figure 5.11**). In light (no Rh, with irradiation) and dark (Rh, no irradiation) controls, only peaks corresponding to the singly (DNA^{1+}) and doubly (DNA^{2+}) charged parent single strands are observed, m/z = 8198.7 and 4100.3 for AB1 and 8213.2 and 4106.9 for AB1-C. Photocleavage samples reveal three new masses in addition to the parent strands at m/z = 3733.7, 4286.8, and 4475.9. These fragments are consistent with the DNA being cleaved only on the AB1-C strand. We assign the cleavage fragment at m/z = 3733.7 as a 12-mer with a 5'-phosphate group and the product at m/z = 4286.8 as a 14-mer with a 3'-phosphate group. These fragments correspond to common DNA cleavage products and clearly indicate scission on the 3'-side of the unpaired base. The final cleavage fragment, appearing at m/z = 4475.9, corresponds to the aforementioned 14-mer with a 3'-2,3-dehydronucleotide in place of a phosphate. Upon sample incubation for 24 h at 23 °C, however, complete conversion of the dehydronucleotide product to the 3'-phosphate fragment is observed, suggesting that the former is a metastable intermediate.

Analogous results are obtained for all abasic sites that are cleaved on the strand containing the unpaired base. The situation changes only slightly for the AB4 assemblies,

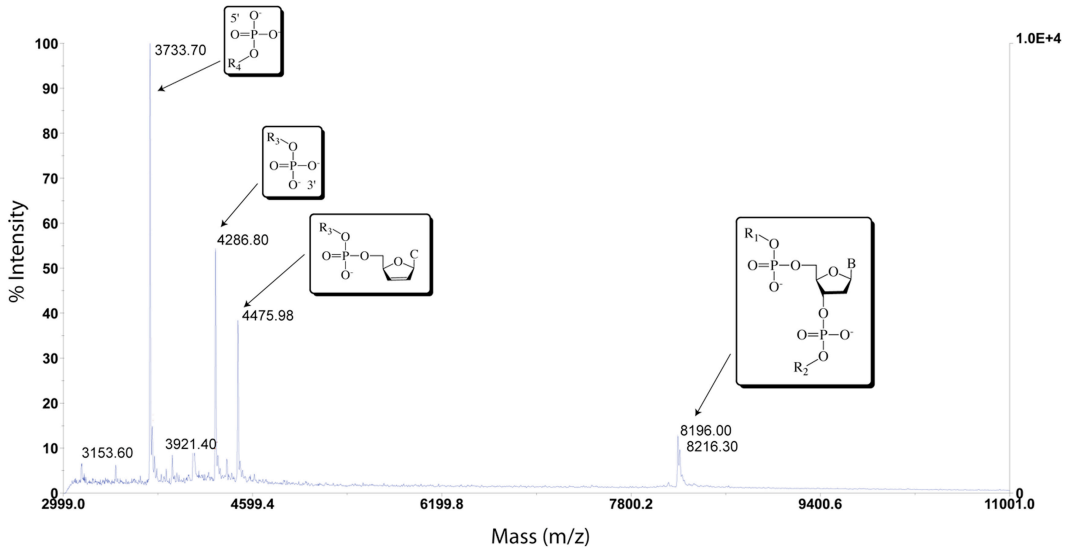

Figure 5.11: Mass spectrometry of abasic site photocleavage products. MALDI-TOF mass spectrograph of photocleavage products of duplex AB1-C, 5'- GAC CAG CTT ATC A*C*C CCT AGA TAA GCG -3' in which the underlined, italicized cytosine is the unpaired complement of an abasic site. The rightmost peaks correspond to the full, uncleaved parent strands. Assigned scission products can be viewed on the left-hand side of the plot and correspond to 5'-PO_4-CCT AGA TAA GCG-3', 5'-GAC CAG CCT ATC A*C*-PO_4-3', and 5'-GAC CAG CCT ATC A*C*-dehydroC-3'. R_1 = GAC CAG CTT ATC A; R_2 = CCC TAG ATA AGC G; R_3 = GAC CAG CCT ATC A*C*; R_4 = CCT AGA TAA GCG; B = cytosine.

in which scission occurs on the strand containing the abasic site; for these duplexes, all of the same cleavage products are observed, but strand scission occurs on the 3' side of the abasic site. Importantly, analogous products are also seen for photocleavage of the mismatched strands. Indeed, exactly the same products are seen for the AB1-C and AB1-MM assemblies (**Figure 5.12)**: strand scission occurs on the 3'-sides of the unpaired cytosine in AB1-C and the corresponding mispaired cytosine in AB1-MM, resulting in identical fragments. Interestingly, unlike previous MALDI-TOF experiments with mismatched sites[18, 63], no furanose products were observed. The same is true for the MALDI-TOF analysis of the abasic assemblies.

Taken together, these mass spectrometry experiments provide a number of key insights. First, the data confirm observations made via gel electrophoresis regarding site specificity, strand asymmetry of scission, and cleavage product length. More important, however, is the light shed on the relationship between the recognition of abasic sites and that of mismatches. As stated above, analogous, and in some cases indistinguishable, products are observed for mismatch and abasic site photocleavage. This result strongly suggests a similar, if not identical, binding mode for metalloinsertors at abasic sites. Furthermore, cleavage product analysis and structural information have indicated that mismatch photocleavage proceeds via an H1'-abstraction mechanism. The results at hand indicate that abasic site strand scission occurs via the same pathway.

5.2.7: Recognition of single base bulges by $Rh(bpy)_2(chrysi)^{3+}$

Compared to abasic sites, single base bulges are recognized less effectively and, when bound, cleaved less efficiently. In fact, out of the sixteen possible single base

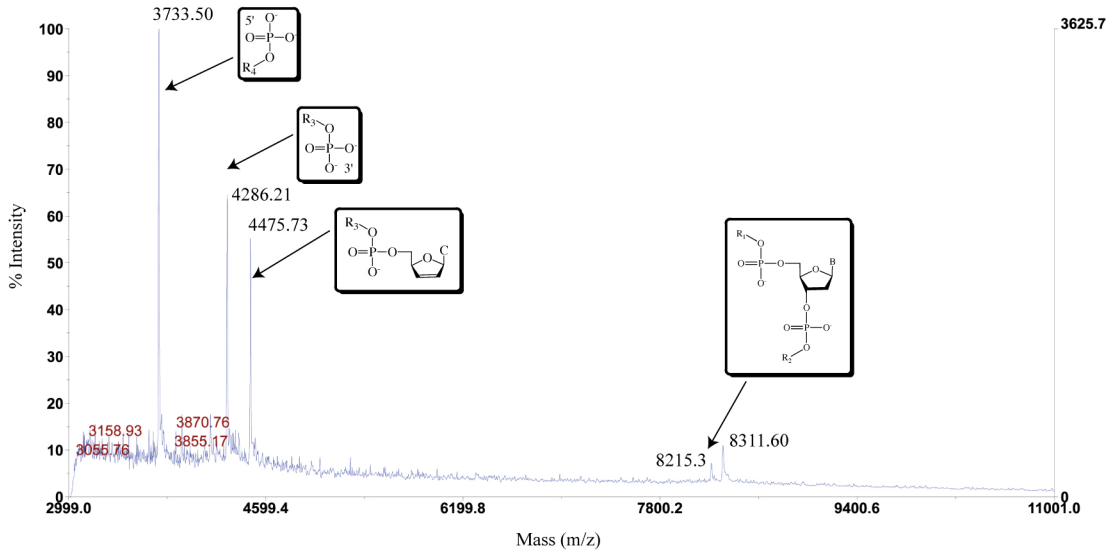

Figure 5.12: Mass spectrometry of mismatch site photocleavage products. MALDI-TOF mass spectrograph of photocleavage products of duplex AB1-MM, 5'- GAC CAG CTT ATC A*C*C CCT AGA TAA GCG -3' in which the underlined, italicized cytosine is the complement of a mismatched C. The rightmost peaks correspond to the full, uncleaved parent strands. Assigned scission products can be viewed on the left-hand side of the plot and correspond to 5'-PO_4-CCT AGA TAA GCG-3', 5'-GAC CAG CCT ATC A*C*-PO_4-3', and 5'-GAC CAG CCT ATC A*C*-dehydroC-3'. R_1 = GAC CAG CTT ATC A; R_2 = CCC TAG ATA AGC G; R_3 = GAC CAG CCT ATC A*C*; R_4 = CCT AGA TAA GCG; B = cytosine.

bulges in this investigation, only seven were recognized and cleaved: B1-C, B1-G, B1-T, B2-A, B2-C, B2-G, and B2-T (**Figure 5.13**). Furthermore, in some cases, even faint bulge photocleavage bands required longer irradiation times (20−30 min, compared to 10 min for substantial abasic site cleavage). Based on comparison to shorter labeled oligonucleotides, the bulge photocleavage fragments appear to be 14 bases long for the B1 duplexes and 15 bases long for the B2 duplexes, indicating strand scission on the 3'-side of the bulged base. However, the low photocleavage efficiency at single base bulges precludes the accurate determination of binding affinities. Based on photocleavage titrations and qualitative observations, however, it is evident that in each case the metalloinsertor binding affinity is ~10^5 M^{-1}.

Both sequence context and bulged base identity appear to play roles in recognition. Single base bulges in the B3 and B4 sequence contexts escape binding and photocleavage *in toto*, whereas all of the bulges in the B2 sequence context are recognized and cleaved to some extent. The recognition of single base bulges in the B1 sequence context seems to be dependent upon the identity of the bulged base; the bulged cytosine, guanine, and thymine are cleaved, whereas the bulged adenine is not. Proffering an explanation for this behavior proves difficult, especially without the aid of simple trends for the thermodynamic destabilization of singe base bulge sites (see DISCUSSION).

Despite the lack of generality in the recognition of single base bulges, the initial photocleavage assays and subsequent experimentation do provide some insight into how the metalloinsertor may bind these sites. First, the strand asymmetry and cleavage product length of single base bulge scission match those of photocleavage at mismatched

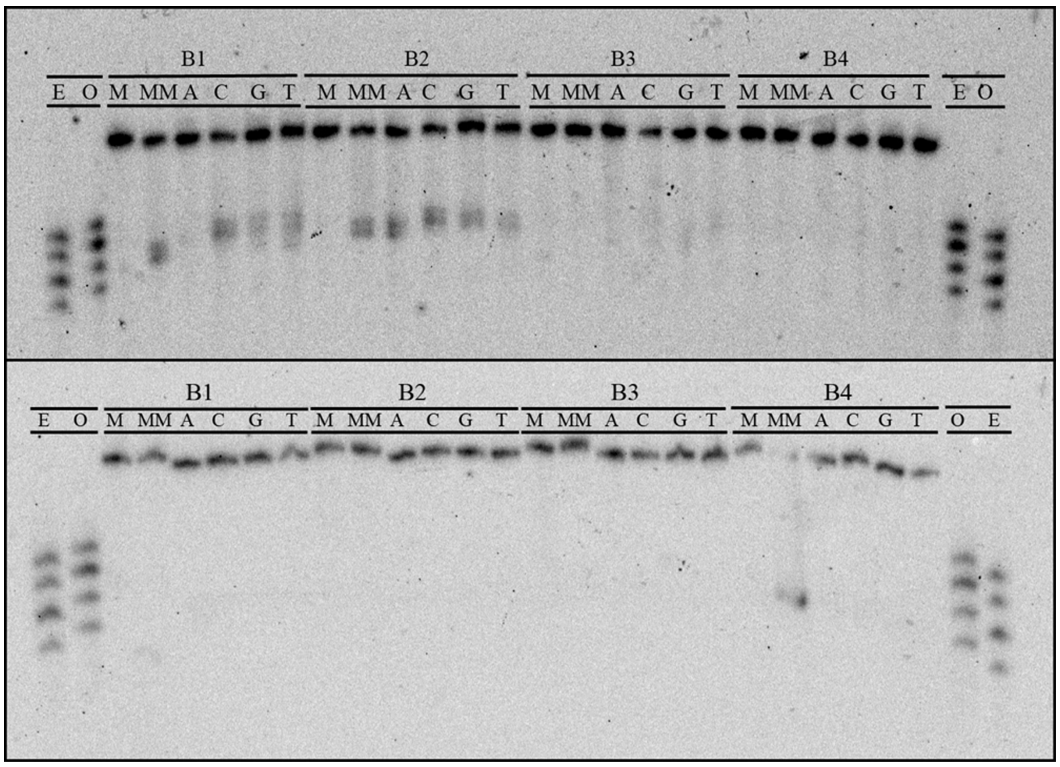

Figure 5.13: Single base bulge recognition and photocleavage gel. PAGE assay illustrating the recognition and photocleavage of mismatch and single base bulge recognition. Sequence contexts are listed along top line of each gel, and individual duplexes are indicated in the second line (M = matched, MM = mismatched, A = bulged adenine, C = cytosine, G = guanine, and T = thymine). In the top gel, the single strand beginning 5'-GAC CAG … (that containing the bulged base in SBB assemblies) is 5'-^{32}P-labeled. In the bottom gel, the single strand beginning 5'-GAC TTA … is 5'-^{32}P-labeled. In both experiments, 1 μM duplex was incubated with $Rh(bpy)_2(chrysi)^{3+}$ in 50 mM NaCl, 10 mM NaPi, pH 7.1. Samples were irradiated for 30 min on an Oriel Instruments solar simulator (320−440 nm emission) and incubated for 30 min at 60 °C prior to electrophoresis. "E" and "O" denote lanes containing even (10, 12, 14, 16) and odd (11, 13, 15, 17) standardization fragments.

sites. Second, photocleavage assays employing Δ- and Λ-$Rh(bpy)_2(chrysi)^{3+}$ clearly indicate that bulge recognition is enantiospecific for the right-handed isomer of the metalloinsertors. Third, MALDI-TOF analysis of bulge photocleavage products reveal fragments analogous to those produced in mismatch and abasic site recognition and scission (**Figure 4.14)**.[1] For example, $Rh(bpy)_2(chrysi)^{3+}$ photocleavage of the B2-A duplex produces fragments of m/z = 7999.9, 8251.1, 3442.7, 4614.8, and 4802.3. The first two values correspond to the parent single strands of the duplex. The peak at m/z = 3442.7 corresponds to an 11-mer fragment with a 5'-phosphate, the fragment at m/z = 4614.8 to a 15-mer with a 3'-phosphate, and that at m/z = 4798.7 to the same 15-mer fragment but with a 3'-2,3-dehydronucleotide instead of a 3'-phosphate. These products are, in fact, almost identical to those produced via cleavage of the AB2-A abasic site. Thus the data clearly suggest that even though $Rh(bpy)_2(chrysi)^{3+}$ only recognizes single base bulges in a minority of cases, lesion binding, when it does happen, likely occurs in a mode analogous to that of the metalloinsertor at mismatches and abasic sites.

5.3: DISCUSSION

$Rh(bpy)_2(chrysi)^{3+}$ recognizes abasic sites with high affinity and specificity and with little regard for sequence context or the identity of the opposing unpaired base. The targeting of single base bulges, however, appears to be more complicated, with only seven of sixteen possible single base bulge sites bound and cleaved by the metal

[1] The low photocleavage efficiency associated with single base bulge photocleavage renders MALDI-TOF analysis difficult owing to the low amounts of product fragments produced; however, all relevant peaks can be easily identified above baseline.

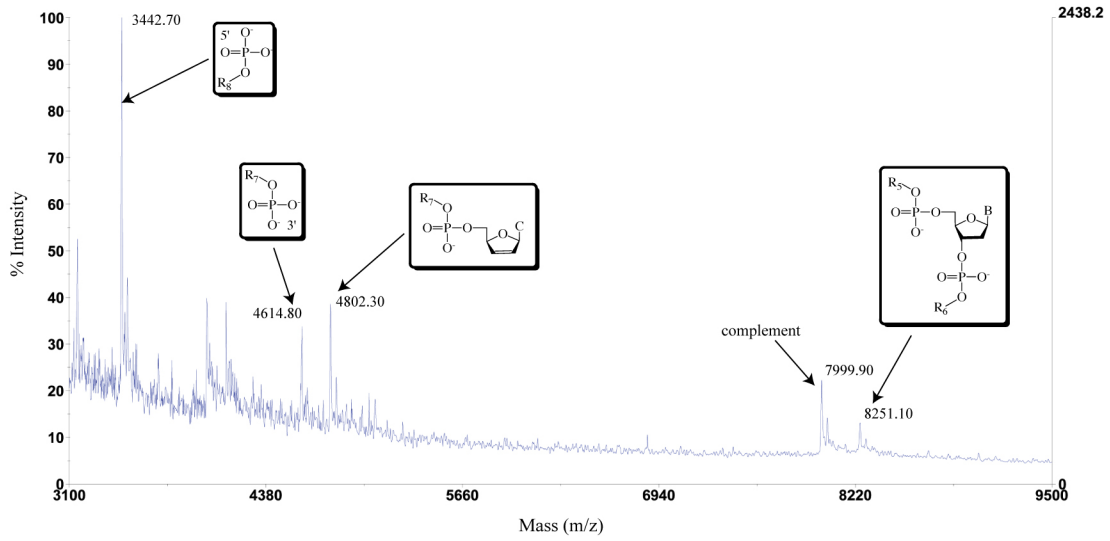

Figure 5.14: Mass spectrometry of single base bulge photocleavage products. MALDI-TOF mass spectrograph of photocleavage products of duplex B2-A, 5'-GAC CAG CTT ATC AT*A* CCT AGA TAA GCG -3' in which the underlined, italicized adenine is the unpaired, bulged base. The rightmost peaks correspond to the full, uncleaved parent strands. Assigned scission products can be viewed on the left-hand side of the plot and correspond to 5'-PO_4-CTA GAT AAG CG-3', 5'-GAC CAG CCT ATC AT*A*-PO_4-3', and 5'-GAC CAG CCT ATC AT*A*-dehydroC-3'. R_5 = GAC CAG CTT ATC AT; R_6 = CCT AGA TAA GCG; R_7 = GAC CAG CCT ATC AT*A*; R_8 = CTA GAT AAG CG; B = Adenine

complex. Yet, now that we have shown that $Rh(bpy)_2(chrysi)^{3+}$ can, indeed, bind both types of site, two simple questions follow: (1) how does the complex bind each lesion and (2) what are the constraints upon the recognition of these defects?

5.3.1: $Rh(bpy)_2(chrysi)^{3+}$ binds abasic sites via metalloinsertion

NMR and X-ray crystallographic evidence has revealed that $Rh(bpy)_2(chrysi)^{3+}$ binds mismatched sites not by classical major groove intercalation but rather via a previously unseen binding mode: insertion. The complex approaches the DNA from the minor groove, ejects the mismatched bases into the major groove, and replaces the extruded bases in the π-stack with its own aromatic ligand (**Figure 5.2**).

In the absence of concrete structural information for the binding mode at abasic sites, we must rely on comparisons to mismatch recognition when considering how $Rh(bpy)_2(chrysi)^{3+}$ targets abasic sites. The similarities are striking. First, photocleavage at mismatches and abasic sites exhibits identical strand asymmetry. In the AB1 and AB2 duplexes, the metal complex cleaves the strand containing the unpaired bases; in the AB4 duplexes, the strand containing the abasic site is cut. Mismatch photocleavage mirrors this behavior, with the corresponding strands of the mismatched duplexes being photocleaved. Second, the enantiospecificity of recognition is revealing. While bis-dipyridyl complexes intercalate into B-DNA with very little enantioselectivity[64], Δ-$Rh(bpy)_2(chrysi)^{3+}$ is able to target and cleave mismatched sites enantiospecifically, a consequence of metalloinsertion occurring from the sterically constrictive minor groove. The same high specificity is observed for the recognition of abasic sites: only the right-handed enantiomer targets and cleaves the abasic lesion. This clearly argues strongly for

involvement of the minor groove. Third, analysis of photocleavage products by mass spectrometry provides still more evidence for similarity. This technique reveals that both abasic sites and mismatches are cleaved on the 3'-side of the defects, producing three products: (1) a fragment containing a 5'-phosphate, (2) a fragment containing a 3'-phosphate, and (3) a metastable fragment identical to (2) but with a 3'-2,3-dehydronucleotide. Indeed, when the unpaired base in the abasic assembly is a cytosine and thus contains the same sequence as the mismatched assembly, identical photocleavage fragments are formed. These products are consistent with H1'-hydrogen abstraction by the photoactivated ligand, a mechanistic pathway accessible only via the minor groove. Finally, a variety of other, more minor similarities between abasic site and mismatch recognition exist, including the failure of $Rh(bpy)_2(chrysi)^{3+}$ to target either type of defect in the AB3 sequence context and the similarity of the site-specific binding affinities of the complex for both types of lesion. These observations also argue for similar binding modes. In sum, this study clearly indicates that the recognition and photocleavage of abasic sites by metalloinsertors occur in a manner almost, if not precisely, identical to mismatch targeting. Thus, these data are fully consistent with $Rh(bpy)_2(chrysi)^{3+}$ targeting abasic sites via metalloinsertion from the minor groove (**Figure 5.15)**. It should be noted that this conclusion fits well with an intuitive and teleological approach to the situation: to a metalloinsertor, an abasic site looks like a mismatch with half the extrusion work already accomplished.

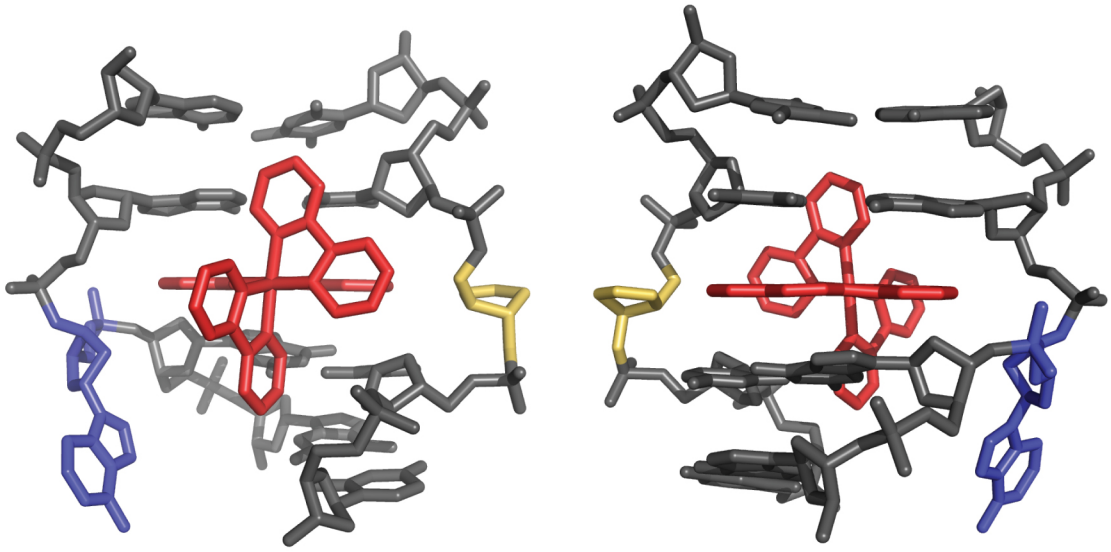

Figure 5.15. Model for metalloinsertion at an abasic site. The metalloinsertor, $Rh(bpy)_2(chrysi)^{3+}$ approaches the abasic site from the minor groove, ejects the unpaired base, and replaces it in the π-stack with the sterically expansive chrysi ligand. Views from the minor (left) and major (right) grooves are shown. The model is based on the crystal structure of $Rh(bpy)_2(chrysi)^{3+}$ inserted at a C•A mismatch.[8]

5.3.2: FACTORS AFFECTING THE RECOGNITION OF ABASIC SITES BY METALLOINSERTORS

Certainly the most puzzling aspect of the investigation into the recognition of abasic sites is the absence of photocleavage for the abasic AB3 duplexes. Neither sequence context nor thermodynamic stabilization provide satisfying explanations; the AB2 duplexes, which also house the abasic site in a 5'-PurΦPur-3' sequence context, are cleaved, and melting temperature measurements suggest that the AB3 duplexes are as destabilized as the other abasic assemblies. The failure of $Rh(bpy)_2(chrysi)^{3+}$ to cleave the AB3 duplex containing a central C•C mismatch is equally, if not more, surprising. Cytosine-cytosine mismatches are among the most destabilizing mispairs and are readily recognized and cleaved by metalloinsertors in almost any sequence context. It follows that the most likely, if slightly unsatisfying, explanation is based purely on sequence: the particular 5'-AΦG-3' sequence context in the AB3 duplexes simply does not allow for efficient binding and photocleavage. Such anomalies, though poorly understood at present, have been reported for mismatch targeting and constitute only a very small percentage of cases.[65]

5.3.3: FACTORS AFFECTING RECOGNITION OF SINGLE BASE BULGES BY METALLOINSERTORS

The somewhat sporadic recognition and cleavage of single base bulges by $Rh(bpy)_2(chrysi)^{3+}$ also merit some attention. As we have noted, only seven of sixteen possible bulges were recognized and cleaved. A thermodynamic rationale is not available, principally due to the lack of reliable, reported patterns between bulge

sequence and destabilization. Sequence context surely plays a role, but it cannot be the sole determining factor. Both the B2 and B3 assemblies place the bulged base in a 5'-PyrXPyr-3' context, but one set of duplexes (B2) exhibits cleavage regardless of bulged base identity, while the other (B3) escapes recognition entirely. The selective cleavage of three bulged bases in the B1 assemblies suggests that the identity of the bulged base may be a determining factor, but the recognition of the B2 sequence bulges regardless of base identity suggests a slightly more complicated rationale.

One possible explanation may be found in the likely conformation of the bulged base. In the B2 duplexes, all of which are photocleaved by $Rh(bpy)_2(chrysi)^{3+}$, each bulged base is in a 5'-PyrXPyr-3' sequence context and is therefore likely to spend at least some time in a extrahelical conformation. In contrast, the B4 duplexes house the bulged base in a 5'-PurXPur-3' conformation, with the better-stacking purines shifting the likely position of the bulged base from extra- to intrahelical; in this case, none of the single base bulges is bound and cleaved. The B1 duplexes provide an intermediate case. Here, the bulged bases are in a 5'-PyrXPur-3' sequence context. In this case, the bulged bases likely in an extrahelical conformation, the pyrimidines C and T, are bound and cleaved, while one of those more likely to prefer an intrahelical orientation, the purine A, escapes recognition. In sum, the data suggest that the more likely a base is to exist in an extrahelical conformation, the more easily it will be targeted by our metalloinsertors. It should be noted, however, that this hypothesis fails to explain the successful targeting of the bulged guanine in the B1-G assembly.

Disregarding the specifics, a more satisfying, if not more vague, explanation for the sporadic recognition of single base bulges can be found in the structure of the sites

themselves. While single base bulges are structurally related to abasic sites, they are not, of course, identical. In the former, the unpaired base lies across from an abasic ribose, and it follows that the bases flanking this sugar are separated by a ribophosphate unit. In the latter, the unpaired base is simply an extra nucleotide inserted into an otherwise well-matched helix: there is no ribophosphate 'space' complementary to the bulge site. These differences take on extra weight when a metalloinsertor binds. At a mismatch, $Rh(bpy)_2(chrysi)^{3+}$ ejects the mispaired bases and replaces them in the DNA π-stack with its sterically expansive ligand; in the end, the chrysi ligand is stacked between two non-adjacent base pairs that are separated on each strand by ribophosphate units connected to the once-mismatched, now-extruded base pairs. The same structure minus one of the extruded nucleobases is adopted during metalloinsertion at an abasic site. However, this type of binding is not possible at a single base bulge. Because there is no empty ribophosphate 'space' across from the bulged base, a metal complex must bind the site via a hybrid metallointercalation/metalloinsertion binding mode. One half of the sterically expansive ligand must bind via intercalation, stacking between adjacent base pairs, while the other half must bind via insertion, extruding the bulged base and taking its place in the π-stack (**Figure 4.16**). Logically, it follows that if the binding mode for the metalloinsertor changes, the rules for recognition and affinity must likewise change. In the end, we believe that this altered binding geometry is responsible for the failure of $Rh(bpy)_2(chrysi)^{3+}$ to reliably recognize and photocleave single base bulges.

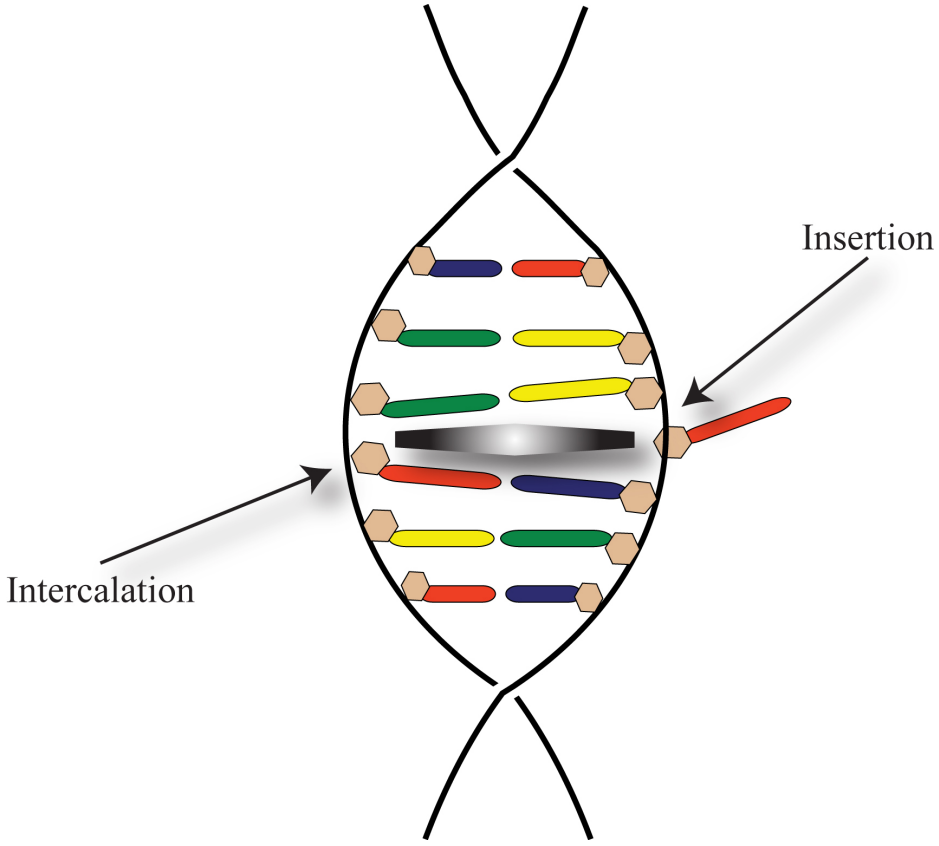

Figure 5.16: The hybrid binding mode required by single base bulges. Because there is no empty ribophosphate 'space' across from the bulged base, a metal complex must bind the site via a hybrid metallointercalation/metalloinsertion binding mode. The left side of the sterically expansive ligand (silver) must bind via intercalation, stacking between adjacent base pairs, while the right half binds must bind via insertion, extruding the bulged base and taking its place in the π-stack

5.4: CONCLUSIONS

This investigation clearly illustrates that both abasic sites and single base bulges are targeted by $Rh(bpy)_2(chrysi)^{3+}$, a sterically bulky metalloinsertor. Abasic sites are targeted with high specificity and affinity in all sequence contexts and with all unpaired bases, and a wide variety of evidence points to metalloinsertion as the binding mode of the complex at these defects. The recognition of single base bulges is less reliable, though the available data suggest an insertion-type binding mode is likely in this case as well.

The broader implications of this study are threefold. The revelation that specific metalloinsertion is not a phenomenon unique to mismatches certainly is important in the development of recognition agents for DNA defects. Perhaps this and subsequent investigations will enable us to expand the utility of these complexes beyond mismatch recognition into applications involving the *in vivo* detection of abasic sites or other thermodynamically destabilized DNA defects. Second, the ability of $Rh(bpy)_2(chrysi)^{3+}$ to specifically target abasic sites represents an exciting diagnostic possibility. A reliable probe for these lesions, especially one with the specificity, affinity, and reactivity of $Rh(bpy)(chrysi)^{3+}$ or $Rh(bpy)_2(phzi)^{3+}$, could prove an invaluable clinical and diagnostic tool. And third, these results dictate that abasic sites and single base bulges may, in addition to mismatches, be *in vivo* targets for metalloinsertors. Experiments with mismatch repair proficient and deficient cell lines have illuminated the substantial therapeutic potential of metalloinsertors and, furthermore, have strongly suggested that $Rh(bpy)_2(chrysi)^{3+}$ and $Rh(bpy)_2(phzi)^{3+}$ target mismatches in the cell. Similar studies employing cells deficient in abasic site repair pathways may further expose the potential therapeutic value of these complexes. Looking forward, the discovery that

metalloinsertors specifically target and photocleave abasic sites creates a variety of new and exciting opportunities in the study and development of metal complexes that target DNA lesions.

5.5: EXPERIMENTAL PROTOCOLS

Many of the procedural details for this investigation are included in CHAPTER 2 of this text. These include the following: the synthesis of $Rh(bpy)_2(chrysi)^{3+}$ and $Rh(bpy)_2(phzi)^{3+}$ (2.3.2.5−2.3.2.6); and the synthesis, purification, and radiolabeling of oligonucleotides (2.4.1−2.4.2). Although general methods for photocleavage gel experiments and MALDI-TOF mass spectrometry are also described in CHAPTER 2, the critical nature of these procedures in this investigation dictates that detailed protocols be presented here as well.

5.5.1: MATERIALS AND INSTRUMENTATION

All reagents were obtained from commercial sources and used as received without further purification. $RhCl_3$ was purchased from Pressure Chemicals. $Rh(bpy)_2(phi)^{3+}$ and $Rh(bpy)_2(chrysi)^{3+}$ were synthesized according to published protocols.[58] The enantiomers of $Rh(bpy)_2(chrysi)^{3+}$ were likewise resolved as described earlier.[58] All non-aqueous solvents were purchased from Fluka and stored under argon and over molecular sieves. All water used was purified using a MilliQ water purification system.

Analytical mass spectrometry was performed at either the Caltech mass spectrometry facility or in the Beckman Institute Protein/Peptide Micro Analytical

Laboratory (PPMAL). Absorption spectra were recorded on a Beckman DU 7400 spectrophotometer.

Standard oligonucleotides were synthesized on an ABI 3400 DNA synthesizer. Abasic site-containing oligonucleotides were ordered from Integrated DNA technologies; given the instability of the natural hemiacetal abasic lesion[59], the often employed tetrahydrofuranyl abasic site analogue was used instead (**Figure 5.4c**).[60, 61] In all text, the symbol Φ denotes the abasic site. Following synthesis or delivery, the oligonucleotides were purified both with and without dimethoxytrityl (DMT) protecting groups via reverse phase HPLC (see Chapter 2, Section 2.4.1).

Concentrations of metal complexes were determined using UV-visible spectrophotometry with extinction coefficients of ε_{302} = 57,000 $cm^{-1}M^{-1}$ and ε_{315} = 52,200 $cm^{-1}M^{-1}$ for $Rh(bpy)_2(chrysi)^{3+}$ and ε_{304} = 65,800 $cm^{-1}M^{-1}$ and ε_{314} = 67,300 $cm^{-1}M^{-1}$ for $Rh(bpy)_2(phzi)^{3+}$. DNA strand concentrations were also determined spectrophotometrically using base extinction coefficients of ε_{260} = 15,400 $cm^{-1}M^{-1}$ (A), ε_{260} = 7,400 $cm^{-1}M^{-1}$ (C), ε_{260} = 11,500 $cm^{-1}M^{-1}$ (G), and ε_{260} = 8,700 $cm^{-1}M^{-1}$ (T). DNA concentrations are presented per strand. Duplex melting temperatures were determined by following hypochromicity at 260 nm for 1 μM duplex in a buffer of 50 mM NaCl, 10 mM NaPi, pH 7.1, via variable temperature UV-Vis.

All oligonucleoties were 5'-radioactively labeled with ^{32}P using [γ-^{32}P]ATP (MP Biomedicals) and polynucleotide kinase (Roche) employing standard methodologies and purified via 20% polyacrylamide gel electrophoresis (SequaGel, National Diagnostics) (see Chapter 2, Section 2.4.2). All photocleavage experiments were performed using end-labeled DNA with identical sequence, unlabeled carrier DNA in a buffer of 50 mM NaCl,

10 mM NaPi, pH 7.1. Duplexes were annealed by incubation at 90 °C for 15 min followed by slow cooling to room temperature.

Irradiations were performed using an Oriel Instruments solar simulator (320−440 nm). All PAGE experiments described employed denaturing 20% polyacrylamide gels (SequaGel, National Diagnostics) and were performed according to published procedures. Gels were developed using Molecular Dynamics phosphorimaging screens and a Molecular Dynamics Storm 820 phosphorimager and were subsequently visualized and quantified with Molecular Dynamics ImageQuant software.

MALDI-TOF mass spectrometry was performed using a Voyager DE-PRO MALDI-TOF mass spectrometer with a 337 nm nitrogen laser source (Applied Biosystems). A 4-hydroxypicolinic acid matrix was employed. All mass spectra were internally calibrated using the mass of the parent oligonucleotide.

5.5.2: RECOGNITION AND PHOTOCLEAVAGE EXPERIMENTS.

Solutions of $Rh(bpy)_2(chrysi)^{3+}$ or $Rh(bpy)_2(phzi)^{3+}$ were incubated with 5'-^{32}P-labeled oligonucleotides either containing or lacking a central DNA lesion (see section 5.3.1 for further details). Unless otherwise noted, final solutions were prepared 20 min prior to irradiation, contained 1 μM duplex and 1 μM metalloinsertor, and were 20 μL in volume. Dark and light control samples, of course, lacked the appropriate solution components. Because metalloinsertor photocleavage is single-stranded, each duplex was interrogated twice, once with each of the two strands radioactively labeled. Samples were irradiated with an Oriel Instruments solar simulator (320−440 nm). Irradiations were performed in open, vertically oriented 1.7 mL microcentrifuge tubes. After irradiation,

samples were incubated at 60 °C for 30 min and then dried under vacuum. Dried samples were redissolved in denaturing formamide loading dye and electrophoresed on 20% denaturing polyacrylamide gels. Images of the gels were obtained via phosphorimagery (Molecular Dynamics) and quantified using ImageQuant software.

5.5.3: DETERMINATION OF SITE-SPECIFIC BINDING CONSTANTS.

Photocleavage titrations were performed to determine the thermodynamic binding constants for $Rh(bpy)_2(chrysi)^{3+}$ with lesion sites of interest. Solutions of DNA (1 μM) were incubated with variable concentrations of $Rh(bpy)_2(chrysi)^{3+}$ (0−20 μM) and subsequently irradiated on an Oriel Instruments solar simulator for 10 min. After irradiation, the samples were incubated at 60 °C for 30 min and then dried under vacuum. Dried samples were redissolved in denaturing formamide loading dye and electrophoresed on 20% denaturing polyacrylamide gels. Images of the gels were obtained via phosphorimagery (Molecular Dynamics). The fraction cleaved at the lesion site was quantitated using ImageQuant software, expressed as a fraction of the total parent DNA, and fit to a single site, one parameter binding model.

5.5.4: MALDI-TOF ANALYIS OF CLEAVAGE PRODUCT

For mass spectrometry analysis of photocleavage products, 2 μM solutions of duplex were incubated with 2 μM $Rh(bpy)_2(chrysi)^{3+}$ and irradiated as described above. After irradiation and incubation, the samples were dried under vacuum, resuspended in 10 μL water, and desalted using 10 μL OMIX C18 tips (Varian). The resultant desalted solution was dried *in vacuo* and resuspended in 2 μL deionized H_2O. Appropriate light and dark controls were also prepared. Experiments were performed using a Voyager DE-

PRO MALDI-TOF mass spectrometer with a 337 nm nitrogen laser source (Applied Biosystems). A 4-hydroxypicolinic acid matrix was employed. All mass spectra were internally calibrated using the mass of the parent oligonucleotide. In the interest of thoroughness, the full data sets for the MALDI-TOF analysis of the photocleavage of abasic sites and single base bulges are included in **Tables 5.3−5.7**.

Duplex	[Rh]	Irradiation	Fragment	Fragment Description	Predicted Mass	Obs. Mass
1MM-1C	-	15 min	5'-CGC TTA TCT AGG GCT GAT AAG CTG GTC	1MM-full	8306.5	8306.2
			5'-GAC CAG CTT ATC ACC CCT AGA TAA GCG	1C-full	8213.4	8213.5
1MM-1C	2 μM	15 min	5'-CGC TTA TCT AGG GCT GAT AAG CTG GTC	1MM-full	8306.5	8311.6
			5'-GAC CAG CTT ATC ACC CCT AGA TAA GCG	1C-full	8213.4	8215.25
			5'-PO_4-CCT AGA TAA GCG	5'-phos-frag	3734.5	3733.5
			GAC CAG CTT ATC AC-PO_4-3'	3'-phos-frag	4287.8	4286.8
			GAC CAG CTT ATC AC-PO_4-dehydroC-3'	3'-DHC-frag	4477.8	4475.7
1ϕ-1A	-	15 min	5'- CGC TTA TCT AGG GϕT GAT AAG CTG GTC	1ϕ-full	8197.5	8196.5
			5'-GAC CAG CTT ATC AAC CCT AGA TAA GCG	1A-full	8237.4	8237.3
1ϕ-1A	2 μM	15 min	5'- CGC TTA TCT AGG GϕT GAT AAG CTG GTC	1ϕ-full	8197.5	8195.5
			5'-GAC CAG CTT ATC AAC CCT AGA TAA GCG	1A-full	8237.4	8233.6
			5'-PO_4-CCT AGA TAA GCG	5'-phos-frag	3734.5	3732.6
			GAC CAG CTT ATC AA-PO_4-3'	3'-phos-frag	4311.8	4309.9
			GAC CAG CTT ATC AA-PO_4-dehydroC-3'	3'-DHC-frag	4501.8	4498.2
1ϕ-1C	-	15 min	5'- CGC TTA TCT AGG GϕT GAT AAG CTG GTC	1ϕ-full	8197.5	8196.0
			5'-GAC CAG CTT ATC ACC CCT AGA TAA GCG	1C-full	8213.4	8213.8
1ϕ-1C	2 μM	15 min	5'- CGC TTA TCT AGG GϕT GAT AAG CTG GTC	1ϕ-full	8197.5	8200.2
			5'-GAC CAG CTT ATC ACC CCT AGA TAA GCG	1C-full	8213.4	8216.3
			5'-PO_4-CCT AGA TAA GCG	5'-phos-frag	3734.5	3733.7
			GAC CAG CTT ATC AC-PO_4-3'	3'-phos-frag	4287.8	4286.8
			GAC CAG CTT ATC AC-PO_4-dehydroC-3'	3'-DHC-frag	4477.8	4475.8
1ϕ-1G	-	15 min	5'- CGC TTA TCT AGG GϕT GAT AAG CTG GTC	1ϕ-full	8197.5	8195.2
			5'-GAC CAG CTT ATC AGC CCT AGA TAA GCG	1G-full	8253.4	8250.6
1ϕ-1G	2 μM	15 min	5'- CGC TTA TCT AGG GϕT GAT AAG CTG GTC	1ϕ-full	8197.5	8194.8
			5'-GAC CAG CTT ATC AGC CCT AGA TAA GCG	1G-full	8253.4	8252.4
			5'-PO_4-CCT AGA TAA GCG	5'-phos-frag	3734.5	3732.9
			GAC CAG CTT ATC AG-PO_4-3'	3'-phos-frag	4327.8	4325.9
			GAC CAG CTT ATC AG-PO_4-dehydroC-3'	3'-DHC-frag	4517.8	4514.8
1ϕ-1T	-	15 min	5'- CGC TTA TCT AGG GϕT GAT AAG CTG GTC	1ϕ-full	8197.5	8198.1
			5'-GAC CAG CTT ATC ATC CCT AGA TAA GCG	1T-full	8228.4	8231.2
1ϕ-1T	2 μM	15 min	5'- CGC TTA TCT AGG GϕT GAT AAG CTG GTC	1ϕ-full	8197.5	8199.4
			5'-GAC CAG CTT ATC ATC CCT AGA TAA GCG	1T-full	8228.4	8230.5
			5'-PO_4-CCT AGA TAA GCG	5'-phos-frag	3734.5	3732.5
			GAC CAG CTT ATC AT-PO_4-3'	3'-phos-frag	4302.8	4300.0
			GAC CAG CTT ATC AT-PO_4-dehydroC-3'	3'-DHC-frag	4492.8	4489.9

Table 5.3: MALDI-TOF data for sequence 1 mismatched and abasic assemblies

Duplex	[Rh]	Irradiation	Fragment	Fragment Description	Predicted Mass	Obs. Mass
2MM-2C	-	15 min	5'-CGC TTA TCT AGG CAT GAT AAG CTG GTC	2MM-full	8290.5	8287.3
			5'-GAC CAG CTT ATC ATC CCT AGA TAA GCG	2C-full	8228.4	8225.3
2MM-2C	2 μM	15 min	5'-CGC TTA TCT AGG CAT GAT AAG CTG GTC	2MM-full	8306.5	8311.6
			5'-GAC CAG CTT ATC ATC CCT AGA TAA GCG	2C-full	8213.4	8215.25
			5'-PO_4-CTA GAT AAG CG	5'-phos-frag	3445.3	3443.5
			GAC CAG CTT ATC ATC-PO_4-3'	3'-phos-frag	4592.0	4288.3
			GAC CAG CTT ATC ATC-PO_4-dehydroC-3'	3'-DHC-frag	4782.0	4777.3
2ϕ-2A	2 μM	15 min	5'-CGC TTA TCT AGG ϕAT GAT AAG CTG GTC	2ϕ-full	8181.5	8183.5
			5'-GAC CAG CTT ATC ATA CCT AGA TAA GCG	2A-full	8252.4	8255.3
2ϕ-2A	2 μM	15 min	5'-CGC TTA TCT AGG ϕAT GAT AAG CTG GTC	2ϕ-full	8181.5	8180.9
			5'-GAC CAG CTT ATC ATA CCT AGA TAA GCG	2A-full	8252.4	8251.6
			5'-PO_4-CTA GAT AAG CG	5'-phos-frag	3445.3	3443.9
			GAC CAG CTT ATC ATA-PO_4-3'	3'-phos-frag	4616.0	4612.8
			GAC CAG CTT ATC ATA-PO_4-dehydroC-3'	3'-DHC-frag	4806.0	4603.7
2ϕ-2C	-	15 min	5'-CGC TTA TCT AGG ϕAT GAT AAG CTG GTC	2ϕ-full	8181.5	8181.0
			5'-GAC CAG CTT ATC ATC CCT AGA TAA GCG	2C-full	8228.4	8227.9
2ϕ-2C	2 μM	15 min	5'-CGC TTA TCT AGG ϕAT GAT AAG CTG GTC	2ϕ-full	8181.5	8182.0
			5'-GAC CAG CTT ATC ATC CCT AGA TAA GCG	2C-full	8228.4	8227.1
			5'-PO_4-CTA GAT AAG CG	5'-phos-frag	3445.3	3443.7
			GAC CAG CTT ATC ATC-PO_4-3'	3'-phos-frag	4592.0	4590.9
			GAC CAG CTT ATC ATC-PO_4-dehydroC-3'	3'-DHC-frag	4782.0	4779.0
2ϕ-2G	-	15 min	5'-CGC TTA TCT AGG ϕAT GAT AAG CTG GTC	2ϕ-full	8181.5	8181.0
			5'-GAC CAG CTT ATC ATG CCT AGA TAA GCG	2G-full	8268.4	8271.7
2ϕ-2G	2 μM	15 min	5'-CGC TTA TCT AGG ϕAT GAT AAG CTG GTC	2ϕ-full	8181.5	8186.7
			5'-GAC CAG CTT ATC ATG CCT AGA TAA GCG	2G-full	8268.4	8274.1
			5'-PO_4-CTA GAT AAG CG	5'-phos-frag	3445.3	3447.9
			GAC CAG CTT ATC ATG-PO_4-3'	3'-phos-frag	4632.0	4635.8
			GAC CAG CTT ATC ATG-PO_4-dehydroC-3'	3'-DHC-frag	4822.0	4825.3
2ϕ-2T	-	15 min	5'-CGC TTA TCT AGG ϕAT GAT AAG CTG GTC	2ϕ-full	8181.5	8184.5
			5'-GAC CAG CTT ATC ATT CCT AGA TAA GCG	2T-full	8243.4	8246.3
2ϕ-2T	2 μM	15 min	5'-CGC TTA TCT AGG ϕAT GAT AAG CTG GTC	2ϕ-full	8181.5	8182.7
			5'-GAC CAG CTT ATC ATT CCT AGA TAA GCG	2T-full	8243.4	8242.0
			5'-PO_4-CTA GAT AAG CG	5'-phos-frag	3445.3	3444.2
			GAC CAG CTT ATC ATT-PO_4-3'	3'-phos-frag	4607.0	4605.3
			GAC CAG CTT ATC ATT-PO_4-dehydroC-3'	3'-DHC-frag	4797.0	4794.6

Table 5.4: MALDI-TOF data for sequence 2 mismatched and abasic assemblies

Duplex	[Rh]	Irradiation	Fragment	Fragment Description	Predicted Mass	Obs. Mass
4MM-4C	-	15 min	5'-CGC TTA TCT AGT CCT GAT AAG CTG GTC	4MM-full	8241.1	8233.9
			5'-GAC CAG CTT ATC AGC ACT AGA TAA GCG	4C-full	8277.5	8272.7
4MM-4C	2 μM	15 min	5'-CGC TTA TCT AGT CCT GAT AAG CTG GTC	4MM-full	8241.1	8244.9
			5'-GAC CAG CTT ATC AGC ACT AGA TAA GCG	4C-full	8277.5	8275.7
			5'-PO_4-TGA TAA GCT GGT C	5'-phos-frag	4069.7	4067.1
			CGC TTA TCT AGT C-PO_4-3'	3'-phos-frag	3980.6	3978.9
			CGC TTA TCT AGT C-PO_4-dehydroC-3'	3'-DHC-frag	4170.6	4166.0
4ϕ-4A	2 μM	15 min	5'-CGC TTA TCT AGT ϕCT GAT AAG CTG GTC	4ϕ-full	8132.3	8130.8
			5'-GAC CAG CTT ATC AGA ACT AGA TAA GCG	4A-full	8302.5	8299.8
4ϕ-4A	2 μM	15 min	5'-CGC TTA TCT AGT ϕCT GAT AAG CTG GTC	4ϕ-full	8132.3	8130.5
			5'-GAC CAG CTT ATC AGA ACT AGA TAA GCG	4A-full	8302.5	8300.2
			5'-PO_4-TGA TAA GCT GGT C	5'-phos-frag	4069.7	4064.1
			CGC TTA TCT AGT ϕ-PO_4-3'	3'-phos-frag	3871.4	3869.0
			CGC TTA TCT AGT ϕ-PO_4-dehydroC-3'	3'-DHC-frag	4061.6	*Buried*
4ϕ-4C	-	15 min	5'-CGC TTA TCT AGT ϕCT GAT AAG CTG GTC	4ϕ-full	8132.3	8129.5
			5'-GAC CAG CTT ATC AGC ACT AGA TAA GCG	4C-full	8277.5	8274.8
4ϕ-4C	2 μM	15 min	5'-CGC TTA TCT AGT ϕCT GAT AAG CTG GTC	4ϕ-full	8132.3	8133.7
			5'-GAC CAG CTT ATC AGC ACT AGA TAA GCG	4C-full	8277.5	8278.3
			5'-PO_4-TGA TAA GCT GGT C	5'-phos-frag	4069.7	4065.1
			CGC TTA TCT AGT ϕ-PO_4-3'	3'-phos-frag	3871.4	3867.9
			CGC TTA TCT AGT ϕ-PO_4-dehydroC-3'	3'-DHC-frag	4061.6	*Buried*
4ϕ-4G	-	15 min	5'-CGC TTA TCT AGT ϕCT GAT AAG CTG GTC	4ϕ-full	8132.3	8131.9
			5'-GAC CAG CTT ATC AGG ACT AGA TAA GCG	4G-full	8317.5	8318.9
4ϕ-4G	2 μM	15 min	5'-CGC TTA TCT AGT ϕCT GAT AAG CTG GTC	4ϕ-full	8132.3	8132.1
			5'-GAC CAG CTT ATC AGG ACT AGA TAA GCG	4G-full	8317.5	8317.0
			5'-PO_4-TGA TAA GCT GGT C	5'-phos-frag	4069.7	4066.2
			CGC TTA TCT AGT ϕ-PO_4-3'	3'-phos-frag	3871.4	3868.3
			CGC TTA TCT AGT ϕ-PO_4-dehydroC-3'	3'-DHC-frag	4061.6	*Buried*
4ϕ-4T	-	15 min	5'-CGC TTA TCT AGT ϕCT GAT AAG CTG GTC	4ϕ-full	8132.3	8131.9
			5'-GAC CAG CTT ATC AGT ACT AGA TAA GCG	4T-full	8292.4	8291.6
4ϕ-4T	2 μM	15 min	5'-CGC TTA TCT AGT ϕCT GAT AAG CTG GTC	4ϕ-full	8132.3	8132.1
			5'-GAC CAG CTT ATC AGT ACT AGA TAA GCG	4T-full	8292.4	8291.1
			5'-PO_4-TGA TAA GCT GGT C	5'-phos-frag	4069.7	4065.5
			CGC TTA TCT AGT ϕ-PO_4-3'	3'-phos-frag	3871.4	3869.4
			CGC TTA TCT AGT ϕ-PO_4-dehydroC-3'	3'-DHC-frag	4061.6	*Buried*

Table 5.5: MALDI-TOF data for sequence 4 mismatched and abasic assemblies

Duplex	[Rh]	Irradiation	Fragment	Fragment Description	Predicted Mass	Obs. Mass
1B-1C	-	15 min	5'-CGC TTA TCT AGG G T GAT AAG CTG GTC	1B-full	8017.5	8019.9
			5'-GAC CAG CTT ATC ACC CCT AGA TAA GCG	1C-full	8213.4	8215.5
1B-1C	2 μM	15 min	5'- CGC TTA TCT AGG G T GAT AAG CTG GTC	1B-full	8017.5	8020.5
			5'-GAC CAG CTT ATC ACC CCT AGA TAA GCG	1C-full	8213.4	8216.6
			5'-PO_4-T AGA TAA GCG	5'-phos-frag1	3156.4	3152.9
			5'-PO_4-CT AGA TAA GCG	5'-phos-frag2	3445.1	3440.7
			GAC CAG CTT ATC ACC C-PO_4-3'	3'-phos-frag	4866.0	4862.4
			GAC CAG CTT ATC ACC C-PO_4-dehydroC-3'	3'-DHC-frag	4058.0	5050.1
2B-2A	2 μM	15 min	5'-CGC TTA TCT AGG AT GAT AAG CTG GTC	2B-full	8000.1	7999.6
			5'-GAC CAG CTT ATC ATA CCT AGA TAA GCG	2A-full	8252.4	8247.9
2B-2A	2 μM	15 min	5'-CGC TTA TCT AGG AT GAT AAG CTG GTC	2B-full	8000.1	7999.9
			5'-GAC CAG CTT ATC ATA CCT AGA TAA GCG	2A-full	8252.4	8251.1
			5'-PO_4-CTA GAT AAG CG	5'-phos-frag	3445.3	3442.7
			GAC CAG CTT ATC ATA-PO_4-3'	3'-phos-frag	4616.0	4614.8
			GAC CAG CTT ATC ATA-PO_4-dehydroC-3'	3'-DHC-frag	4806.0	4798.7
2B-2C	-	15 min	5'-CGC TTA TCT AGG AT GAT AAG CTG GTC	2B-full	8000.1	7998.5
			5'-GAC CAG CTT ATC ATC CCT AGA TAA GCG	2C-full	8228.4	8225.8
2B-2C	2 μM	15 min	5'-CGC TTA TCT AGG AT GAT AAG CTG GTC	2B-full	8000.1	7996.1
			5'-GAC CAG CTT ATC ATC CCT AGA TAA GCG	2C-full	8228.4	8222.7
			5'-PO_4-TAG ATA AGC G	5'-phos-frag1	3156.4	3156.5
			5'-PO_4-C TAG ATA AGC G	5'-phos-frag2	3445.3	3445.8
			GAC CAG CTT ATC ATC C-PO_4-3'	3'-phos-frag	4881.0	4876.9
			GAC CAG CTT ATC ATC C-PO_4-dehydroC-3'	3'-DHC-frag	5073.0	5068.0
2B-2G	-	15 min	5'-CGC TTA TCT AGG AT GAT AAG CTG GTC	2B-full	8000.1	7997.3
			5'-GAC CAG CTT ATC ATG CCT AGA TAA GCG	2G-full	8268.4	8263.4
2B-2G	2 μM	15 min	5'-CGC TTA TCT AGG AT GAT AAG CTG GTC	2B-full	8000.1	7999.7
			5'-GAC CAG CTT ATC ATG CCT AGA TAA GCG	2G-full	8268.4	8266.6
			5'-PO_4-CTA GAT AAG CG	5'-phos-frag	3445.3	3447.2
			GAC CAG CTT ATC ATG-PO_4-3'	3'-phos-frag	4632.0	4632.8
			GAC CAG CTT ATC ATG-PO_4-dehydroC-3'	3'-DHC-frag	4822.0	4820.6
2B-2T	-	15 min	5'-CGC TTA TCT AGG AT GAT AAG CTG GTC	2B-full	8000.1	8002.5
			5'-GAC CAG CTT ATC ATT CCT AGA TAA GCG	2T-full	8243.4	8244.8
2B-2T	2 μM	15 min	5'-CGC TTA TCT AGG AT GAT AAG CTG GTC	2B-full	8000.1	7999.8
			5'-GAC CAG CTT ATC ATT CCT AGA TAA GCG	2T-full	8243.4	8241.5
			5'-PO_4-CTA GAT AAG CG	5'-phos-frag	3445.3	3442.8
			GAC CAG CTT ATC ATT-PO_4-3'	3'-phos-frag	4607.0	4602.3
			GAC CAG CTT ATC ATT-PO_4-dehydroC-3'	3'-DHC-frag	4797.0	4795.6

Figure 5.6: MALDI-TOF data for single base bulge assemblies. Note the evidence for cleavage at "slipped" bulges in 1B-1C and 2B-2C

5.6: REFERENCES

1. Marnett, L. J.; Plastaras, J. P. *Trends in Genetics* **2001**, *17*, 214−221.
2. Loeb, L. A.; Loeb, K. R. *Proceedings of the National Academy of Sciences U. S. A.* **2003**, *100*, 776−781.
3. Li, G. M. *Frotiers in Bioscience* **2003**, *8*, D997−U1.
4. Lyer, R. R.; Pluciennik, A.; Burdett, V.; Modrich, P. L. *Chemical Reviews* **2006**, *106* (2), 302−323.
5. Modrich, P. *Journal of Biological Chemistry* **2006**, *281* (41), 30305−30309.
6. David, S. S.; O'Shea, V. L.; Kundu, S. *Nature* **2007**, *447*, 941−950.
7. Jacob, S.; Praz, F. *Biochemie* **2002**, *84*, 27−47.
8. Kolodner, R. D. *Trends in Biochemical Science* **1995**, *20*, 397−401.
9. Kolodner, R. *Genes & Development* **1996**, *10* (12), 1433−1442.
10. Jiricny, J. *Cancer Surveys* **1996**, *28*, 47−68.
11. Zeglis, B. M.; Pierre, V. C.; Barton, J. K. *Chemical Communications* **2007**, 4565−4579.
12. Jackson, B. A.; Barton, J. K. *Journal of the American Chemical Society* **1997**, *119* (52), 12986−12987.
13. Junicke, H.; Hart, J. R.; Kisko, J. L.; Glebov, O.; Kirsch, I. R.; Barton, J. K. *Proceedings of the National Academy of Sciences U. S. A.* **2003**, *100*, 3737−3742.
14. Jackson, B. A.; Alekseyev, V. Y.; Barton, J. K. *Biochemistry* **1999**, *38* (15), 4655−4662.
15. Jackson, B. A.; Barton, J. K. *Biochemistry* **2000**, *39* (20), 6176−6182.

16. Jackson, B. A.; Henling, L. M.; Barton, J. K. *Inorganic Chemistry* **1999**, *38* (26), 6218−6224.

17. Cordier, C.; Pierre, V. C.; Barton, J. K. *Journal of the American Chemical Society* **2007**, *129*, 12287−12295.

18. Pierre, V. C.; Kaiser, J. T.; Barton, J. K. *Proceedings of the National Academy of Sciences U. S. A.* **2007**, *103*, 429−434.

19. Lhomme, J.; Constant, J. F.; Demeunynck, M. *Biopolymers* **1999**, *52* (2), 65−83.

20. Boiteux, S.; Guillet, M. *DNA Repair* **2004**, *3*, 1−12.

21. Lindahl, T.; Nyberg, B. *Biochemistry* **1972**, *11* (19), 3610−3518.

22. Wilde, J. A.; Bolton, P. H.; Mazumder, A.; Manoharan, M.; Gerlt, J. A. *Journal of the American Chemical Society* **1989**, *111* (5), 1894−1896.

23. Goljer, I.; Kumar, S.; Bolton, P. H. *Journal of Biological Chemistry* **1995**, *270*, 22980−22987.

24. Coppel, Y.; Berthet, N.; Coulombeau, C.; Garcia, J.; Lhomme, J. *Biochemistry* **1997**, *36*, 4817−4830.

25. Feig, M.; Zacharias, M.; Pettitt, B. M. *Biophysical Journal* **2001**, *81*, 351−370.

26. Chen, J.; Dupradeau, F.−Y.; Case, D. A.; Turner, C. J.; Stubbe, J. *Nucleic Acids Research* **2008**, *36* (1), 253−262.

27. Hoehn, S. T.; Turner, C. J.; Stubbe, J. *Nucleic Acids Research* **2001**, *29* (16), 3413−3423.

28. Kalnik, M. W.; Chang, C. N.; Johnson, F.; Grollman, A. P.; Patel, D. J. *Biochemistry* **1989**, *28*, 3373−3383.

29. Vesnaver, G.; Chang, C. N.; Eisenberg, M.; Grollman, A. P.; Breslauer, K. J. *Proceedings of the National Academy of Sciences U. S. A.* **1989**, *86*, 3614−3618.

30. Gelfand, C. A.; Plum, G. E.; Grollman, A. P.; Johnson, F.; Breslauer, K. J. *Biochemistry* **1998**, *37*, 7321−7327.

31. Alani, E.; Chi, N. W.; Kolodner, R. D. *Genes and Development* **1995**, *9*, 234−247.

32. Tanaka, F.; Kameda, A.; Tamamoto, M.; Ohuchi, A. *Biochemistry* **2004**, *43*, 7143−7150.

33. LeBlanc, D. A.; Morden, K. M. *Biochemistry* **1991**, *30*, 4042−4047.

34. Nikonowicz, E. P.; Meadows, R. P.; Gorenstein, D. G. *Biochemistry* **1990**, *25*, 7456−7464.

35. Hare, D.; Shapiro, L.; Patel, D. J. *Biochemistry* **1987**, *25*, 7456−7464.

36. Joshua−Tor, L.; Frolow, F.; Appella, E.; Hope, H.; Rabinovich, D.; Sussman, J. L. *Journal of Molecular Biology* 1992, *225* (2), 397−431.

37. Joshua−Tor, L.; Rabinovich, D.; Hope, H.; Frolow, F.; Appella, E.; Sussman, J. L. *Nature* **1988**, *334*, 82−84.

38. Patel, D. J.; Kozlowski, S. A.; Marky, L. A.; Rice, J. A.; Broka, C.; Itakura, K.; Breslauer, K. J. *Biochemistry* **1982**, *21*, 445−451.

39. Kalnik, M. W.; Norman, D. G.; Swann, P. F.; Patel, D. J. *Journal of Biological Chemistry* **1989**, *264* (7), 3702−3712.

40. Kalnik, M. W.; Norman, D. G.; Zagorski, M. G.; Swann, P. F.; Patel, D. J. *Biochemistry* **1989**, *28*, 294−303.

41. Miller, M.; Harrison, R. W.; Wlodawer, A.; Appella, E.; Sussman, J. L. *Nature* **1988**, *334*, 85−86.

42. Cline, S. D.; Jones, W.; Stone, M. P.; Osheroff, N. *Biochemistry* **1999**, *38*, 15500−15507.

43. Streisinger, G.; Owen, J. *Genetics* **1985**, *109*, 633−659.

44. Shinmura, K.; Tao, H.; Goto, M.; Igarashi, H.; Taniguchi, T.; Maekawa, M.; Takezaki, T.; Sugimura, H. *Carcinogenesis* **2004**, *25* (12), 2311−2317.

45. WIlson, D. M.; Bohr, V. A. *DNA Repair* **2007**, *6*, 544−559.

46. Fkyerat, A.; Demeunynck, M.; Constant, J. F.; Michon, P.; Lhomme, J. *Journal of the American Chemical Society* **1993**, *115*, 9952−9959.

47. Boturyn, D.; Boudali, A.; Constant, J. F.; Defrancq, E.; Lhomme, J. *Tetrahedron* **1997**, *53* (15), 5485−5492.

48. Kobori, A.; Murase, T.; Suda, H.; Saito, I.; Nakatani, K. *Bioorganic & Medicinal Chemistry Letters* **2004**, *14* (13), 3431−3433.

49. Nakatani, K.; Sando, S.; Saito, I. *Journal of the American Chemical Society* 2000, *122*, 2172−2177.

50. Takei, F.; Suda, H.; Hagihara, M.; Zhang, J. H.; Kobori, A.; Nakatani, K. *Chemistry−a European Journal* **2007**, *13* (16), 4452−4457.

51. Cheng, C. C.; Kuo, Y. N.; Chuang, K. S.; Luo, C. F.; WAng, W. J. *Angewandte Chemie−International Edition* **1999**, *38*, 1255−1257.

52. Morgan, J. L.; Buck, D. P.; Turley, A. G.; Collins, J. G.; Keene, F. R. *Journal of Biological Inorganic Chemistry* **2006**, *11* (7), 824−834.

53. Morgan, J. L.; Buck, D. P.; Turley, A. G.; Collins, J. G.; Keene, F. R. *Inorganica Chimica Acta* **2006**, *359* (3), 888−898.

54. Jones, G. B.; Lin, Y. Q.; Ma, D.; Xiao, Z. W.; Hwang, G. S.; Kappen, L.; Goldberg, I. H. *Current Topics in Medicinal Chemistry* **2008**, *8* (6), 436−447.

55. Kappen, L. S.; Goldberg, I. H. *Biochemistry* **1997**, *36* (48), 14861−14867.

56. Kappen, L. S.; Xi, Z.; Goldberg, I. H. *Biochemistry* **2001**, *40* (50), 15378−15383.

57. Xiao, Z.; Kappen, L. S.; Goldberg, I. H. *Bioorganic & Medicinal Chemistry Letters* **2006**, *16* (11), 2895−2899.

58. Zeglis, B. M.; Barton, J. K. *Nature Protocols* **2007**, *2* (2), 357−371.

59. Lindahl, T.; Andersson, A. *Biochemistry* **1972**, *11* (19), 3618−3623.

60. Takeshita, M.; Chang, C. N.; Johnson, F.; Will, S.; Grollman, A. P. *Journal of Biological Chemistry* **1987**, *262*, 10171−10179.

61. Sagi, J.; Hang, B.; Singer, B. *Chemical Research in Toxicology* **1999**, *22*, 917−923.

62. Barton, J. K. *Science* **1986**, *233*, 727−732.

63. Brunner, J.; Barton, J. K. *Journal of the American Chemical Society* **2006**, *128* (21), 6772−6773.

64. Erkkila, K. E.; Odom, D. T.; Barton, J. K. *Chemical Reviews* **1999**, *99* (9), 2777−2795.

65. Jackson, B. A. California Institute of Technology, Pasadena, **2001**.